Resiliencia y estabilidad de redes de potencia usando el modelo de Kuramoto

Cristian Camilo Galindo González

Universidad Nacional de Colombia - Sede Manizales.
Facultad de ingeniería y arquitectura.
Departamento de ingeniería eléctrica, electrónica y computación.
Manizales, Colombia.
2020

Resilience and stability of power grids using the Kuramoto model

Cristian Camilo Galindo González

Thesis submitted as a partial requirement to receive the grade of:
Master in Engineering - Industrial Automation

Advisor:
Ph.D. Gustavo Adolfo Osorio Londoño

Co-advisor:
Ph.D. David Angulo García

Research group:
Percepción y control inteligente (PCI).

Universidad Nacional de Colombia - Sede Manizales.
Facultad de ingeniería y arquitectura. Departamento de ingeniería eléctrica, electrónica y computación.
Manizales, Colombia
2020

To my family for their constant support and my friends at the combo for the laughs and beers.

"We have developed speed, but we have shut ourselves in. Machinery that gives abundance has left us in want. Our knowledge has made us cynical; our cleverness, hard and unkind. We think too much and feel too little. More than machinery we need humanity. More than cleverness we need kindness and gentleness. Without these qualities, life will be violent and all will be lost..."

Charles Chaplin - 1940

Acknowledgements

First and foremost, I would like to thank my advisors Pd.D. Gustavo Adolfo Osorio Londoño and Ph.D. David Angulo García for their amazing contribution to this research, without them this work would have never been possible.

Thanks to Ph.D. Fabiola Angulo García and Ph.D. Jorge Fernando Gutiérrez Gómez for our fruitful discussions and for providing magnificent input to the theoretical understanding of the research problem.

Thanks to M.Eng. Reinel Tabares Soto for expending copious amounts of time in helping us to run some simulations as well as providing a substantial amount of the computational power required.

Thanks to Ph.D. Guillermo Gallo Hernández for teaching me important concepts about numerical simulation which were essential for the development of this work.

Thanks to my partners at *"Physics, Chemistry and Mathematics - Computational Applications (PCM-CA)"* research group and Ph.D. Elisabeth Restrepo Parra for all the great things I learned from all of you throughout the years.

Special thanks to Hypernet Labs and the project Galileo, for supplying a substantial part of the computational resources that were required [1].

This research was supported by *Universidad Nacional de Colombia - Manizales, Dirección de Investigación y Extensión (DIMA)* and *Ministerio de Ciencia, Tecnología e Innovación (Minciencias)* through the projects:

- *"Análisis de la eficiencia de convertidores electrónicos de potencia en aplicaciones de generación de energía eléctrica, a partir de fuentes no convencionales"* under the contract FP44842 - 052 - 2016.
- *"Convocatoria 775: Jóvenes Investigadores e Innovadores por la paz - 2017. Diseño y construcción de un sistema de generación de energía solar fotovoltaica, autónomo y de alta eficiencia con aplicaciones en la zona rural"* under the contract FP44842 - 505 - 2017.

Abstract

In this document, a methodology is developed to test the non-linear stability of the synchronous state in a power grid as well as its resilience to structural failures by applying a percolation-inspired algorithm based in link and node removal simulations. Vulnerability measures are defined in terms of either dynamical or topological features of the power grid and both methods are compared. A basic analysis of the Colombian power grid is also included and used to test the proposed algorithm.

Keywords: Kuramoto model, power grid, synchronization, non-linear dynamics, basin stability, complex network

Resumen

En este documento, se desarrolla una metodología para estudiar la estabilidad no lineal del estado sincronizado en una red de potencia, así como la resiliencia de la misma ante fallas estructurales aplicando un algoritmo inspirado en la percolación en simulaciones de remoción de conexiones y nodos. Se definen medidas de vulnerabilidad en términos de las características topológicas y dinámicas del sistema de potencia y se comparan ambos métodos. Se presenta además un análisis básico del sistema de transmisión de Colombia y se usa como caso particular de estudio para desarrollar las pruebas del algoritmo propuesto.

Palabras clave: Modelo de Kuramoto, red de potencia, sincronización, dinámica no lineal, estabilidad del dominio de atracción, redes complejas

List of Figures

List of Tables

Content

1. Introduction

The emergence of synchronization in systems of agents, coupled through local interactions, is a widely studied phenomenon with multiple applications in physics, biology, and social sciences [5, 6, 7]. In particular, the optimal functioning of a power grid, which represents one of the most complex interacting systems in engineering, highly depends on its ability to maintain a synchronous operation over time despite external disturbances; losing that synchrony, even locally, may lead to cascading failures and complete blackout of the network [8, 9, 10]. Two main concerns have motivated the discussion around dynamical analysis and design of power grids in the last years: the first is the strong economical and social impact that a power outage could cause in the highly electricity-dependant modern society [11]; for instance, the blackout registered across north-east of United States in August 2003, and which affected about 55 million people, was estimated to cost roughly 1100 million USD [12]. The second is the slow transition to renewable energy sources that is being promoted all around the world [13, 14], since it is known that renewable and small power producers have negligible inertia, which imposes instability risks in the power grids [15]. It is worth mentioning that, in particular, Colombia plans to expand the renewable power generation by 2250 MW by 2022 [16].

Network science is a discipline related to statistical physics that intends to explain interesting phenomena observed on large interconnected systems by analysing the fundamental structure of those connections and the neighbour-to-neighbour dynamical interactions, and although it has been successful in the theoretical sense, there is still a huge gap between these approaches and the practical engineering application due to the massive simplifications that those models usually include [17], however, it is still believed that the particular study of power grids is a matter that transcends multiple disciplines [18]. The present work aims to contribute to the development of network science applied to the analysis of power grids stability, and as such, presents an oversimplified model and methodology based on computational physics and synchronization phenomena, which could bring new insights about phenomena observed in real systems, but that can not be considered a thorough review of the power systems engineering literature.

Multiple models have been proposed for the analysis of synchronization in power grids, and they differ mainly in the way loads, power generators and transmission lines are modeled [4]. Probably the most common model is the one called *synchronous motor*, where both, generators and consumers are represented by second-order synchronous machines [19]. This

model is essentially equivalent to the celebrated Kuramoto model when inertia terms are considered [20, 21, 22]. Self-synchronization behaviour of this model occurs when the interactions between connected oscillators are sufficiently strong to overcome the dissimilarity in the ensemble [8, 23, 24, 25].

Recently, the scientific community has put a lot of effort into trying to determine the topological features of the network that can enhance or undermine the non-linear stability of a power grid, that is, its capability to reject finite-size disturbances [26]. This has been approached by energy barrier functions [27, 28, 29] and the basin stability concept [3, 30, 31, 32, 33, 34]. Some interesting findings that deserve to be mentioned, as they provide great insights about the relationship between topology and dynamical stability include: the poor basin stability usually detected on dead-tree arrangements [30], the strong stability found on triangle-shaped motifs [35], the enhanced non-linear stability achieved by increasing global redundancy in the connections [36] or by adding small cyclic motifs [29], the lower basin stability exhibited in general by high-power generator nodes [37], the poor transient behaviour due to highly connected nodes [3], the variation in transient excursion for finite-size disturbances depending on resistance centrality metrics [38, 39], the diminished size of the basin of attraction as well as the appearance of solitary synchronous states when losses are considered in the network [40] and the interplay between inertia and the correlation time of stochastic noise that yield an escape from the basin of attraction [41].

Other studies have focused on estimating the resilience of the complex network against cascading failures [10, 42, 43], the robustness in the transient behavior after localized disturbances [44] and their diffusion through the interconnected system [15], the optimal design of weights and frequencies [45], as well as the identification of key elements in the network that require a control action [46].

Percolation is a theory that takes ideas from statistical physics to study the phase transition from scattered clusters to large-scale connectivity in systems of interacting elements arranged in either lattices or complex networks [47], focusing usually on finding the structural-based thresholds that allow for the propagation of information throughout the system [48, 49], which makes it suitable for the analysis of the topology of power grids [50, 51].

In the present work, a percolation-inspired method is presented in order to evaluate the resilience of a power grid against random and focalized non-local disturbances. By defining a vulnerability measure in terms of the dynamical properties of both, nodes and edges, it is found that attacks that focus on the weakest components of the network can easily provoke cascading failures that lead to total blackout faster than random attacks. The general stability of the power grid is thus analysed in terms of the ability of the nodes to reject finite-size disturbances without losing the synchronous state, as well as the load observed

on each transmission line, which is abstracted from the phase difference between the connected pair of nodes. The criterion of linear stability around the equilibrium point is also consistently used to quickly identify whether a network topology is capable of maintaining the synchronized state or not. Test cases chosen for this study include randomly generated power grids and the Colombian transmission network.

A very similar work can be found in [52], where the authors use centrality measures, namely, the node degree, clustering coefficient and betweenness centrality, to estimate the vulnerability of a node and then proceed to remove the weakest nodes to observe the evolution of the giant component in the network as a function of the number of remaining nodes in the whole graph. Moreover in [53], the elimination process of transmission lines based on betweenness centrality and a random selection are compared. This structural approach to quantify the node vulnerability is considered fundamentally relevant but limited in the sense that dynamical features of the system are ignored; resilience assessments should contemplate topology, dynamics and failure modelling [54]. In [55], besides performing topologically-focused attacks, a procedure is included to account for the recovery of nodes after its failure, yet it does not consider the state evolution through differential equations.

These topological-based methods will be also used in this work to compare the results of removal methods based on dynamical measurements. Other relevant works have to be mentioned; for instance, based on the statistical physics description of networks, some basic percolation properties for different networks have been analysed using generating functions [56], the mean-field approach has been used to build phase diagrams of the connected and disconnected states of networks in terms of their construction parameters [57], the lifetime and reliability of networks has been estimated by setting some probability distributions for node failures [58], analytical performance measures have been developed and tested over structural and dynamical perturbations of the complex system [59], and the propagation of cascading failures through the power transmission or communication architecture of smart grids has also been modelled as a random percolation process [60] or as a continuous phase transition [61]. Besides, in [62], the minimum cut-set (MCS) strategy is used to describe the vulnerability of the components based on the power flow routing, and attacks focused on this MCS are compared to topological vulnerability measurements.

The rest of this document is organized as follows: Chapter 2 starts defining some basic concepts about complex network analysis, then a classical power grid model is derived and translated to the very well-known second-order Kuramoto model, which will be used later to analyse synchronization problems in power grids. Said chapter ends by introducing an algorithm for the generation of graphs that represent closely the characteristics of real-world power grids, which will allow us to construct test cases for later dynamical analysis, as well as an algorithm for the classification of nodes in tree-like graph structures. Chapter 3 formulates

the problem of synchronization dynamics in the Kuramoto model and depicts some common methods and results found in the literature to analyse linear and non-linear stability of the frequency synchronized state in a power grid. Chapter 4 proposes an algorithm for resilience assessment, applies it to synthetic power grids, and presents results on how the structure of the graph and general stability changes throughout the attacking scheme. Chapter 5 then uses the theory and methods previously introduced, to the analysis of the resilience and stability in the Colombian power transmission network. Chapter 6 presents some concluding remarks and future work. Finally, Appendix A elaborates on the applicability of the Kuramoto model and Appendix B gives more detail about the numerical experiments performed.

2. A Dynamical Model for Power Grids

2.1. Abstract

This chapter introduces the simplified model used to describe the dynamical behaviour of a power grid, which will be used in further analysis to test stability and synchronization phenomena. The derived model will be identical to the well known second-order Kuramoto model, vastly studied in the field of many-body physics. Power grids will be represented by graphs and some tools from the framework of complex network analysis will be employed, thus the first section introduces those important concepts that will be constantly cited throughout this document.

2.2. Centrality in Complex Networks

Let us define a *graph* as a tuple $G(\vartheta, \varepsilon)$, where $\vartheta = \{1, 2, ..., N\}$ is a set of nodes and $\varepsilon = \{(i, j),\ \forall i, j \in \vartheta\} \subset \vartheta \times \vartheta$ is a set of edges with cardinality $|\varepsilon| = M$. It is also convenient to define some common concepts used in the analysis of complex networks and that will be addressed later in this document:

- *Adjacency matrix* A: A matrix that represents the connectivity of the network; in particular, for weighted graphs, each element a_{ij} of A will be equal to some weight $w_{ij} \neq 0$ if there is an edge between the nodes i and j and 0 otherwise. Formally, $A = \{a_{ij}\},\ A \in \mathbb{R}^{N \times N}, a_{ij} \in \mathbb{R}$, where:

$$a_{ij} = \begin{cases} w_{ij} \neq 0 & \text{if } (i, j) \in \varepsilon \\ 0 & \text{otherwise} \end{cases} \tag{2-1}$$

- *Oriented incidence matrix* B: Its a matrix where each row represents a node and each

column an edge, specifically, $B = \{b_{ij}\},\ B \in \mathbb{R}^{N\times M}, b_{ij} \in \mathbb{R}$, with:

$$b_{ij} = \begin{cases} 1 & \text{if node } i \text{ incides in edge } j \\ -1 & \text{if edge } j \text{ incides in node } i \\ 0 & \text{otherwise} \end{cases} \tag{2-2}$$

This representation applies to directed graphs, and although the graphs that will be used in this work are undirected, it will be clear in chapter 3 that a direction for the edge construction can still be assumed without loss of generality for our specific application.

- *Laplacian matrix* L: This matrix provides relevant information about the topology of the graph, it is defined as:

$$L = diag(\sum_{j=1}^{n} a_{ij}) - A \tag{2-3}$$

with $L \in \mathbb{R}^{N\times N}$.

- *Degree centrality* $d_k^{(i)}$: Amount of nodes to which node i is connected, normalized by the maximum possible degree in the network. It can be computed as:

$$d_k^{(i)} = \frac{\hat{d}_i}{N-1} \tag{2-4}$$

where $\hat{d}_i = \sum_j^N a_{ij}$.

- *Clustering coefficient* $c_k^{(i)}$: Number of triangles (T_i) in which node i is involved, normalized by the maximum possible amount of such triangles [63], that is:

$$c_k^{(i)} = \frac{2T_i}{\hat{d}_i(\hat{d}_i - 1)} \tag{2-5}$$

- *Node betweenness centrality* $b_k^{(i)}$: Sum of the shortest paths between every pair of nodes (s,t) in the network that pass through node i:

$$b_k^{(i)} = \sum_{s\neq t\neq i\in\vartheta} \frac{\sigma_{s,t}(i)}{\sigma_{s,t}} \tag{2-6}$$

where $\sigma_{s,t}$ is the amount of shortest paths between nodes s and t and $\sigma_{s,t}(i)$ is the number of those paths that pass through node i [64].

- *Edge betweenness centrality* $e_k^{(l)}$: In the same fashion as b_k measures centrality for a node, e_k does it for an edge; it is simply defined as the number of shortest paths in the network that include the edge l:

$$e_k^{(l)} = \sum_{s \neq t \in \vartheta} \frac{\sigma_{s,t}(l)}{\sigma_{s,t}}, \quad l \in \varepsilon \tag{2-7}$$

2.3. Power Grids as Complex Networks

As a simplified model of a real-world power grid, consider a system of N interacting synchronous machines arranged in a connected graph $G(\vartheta, \varepsilon)$, with a set of nodes $\vartheta = \{1, 2, ..., N\}$ and a set of edges $\varepsilon \subset \vartheta \times \vartheta$, such that the amount of edges is $|\varepsilon| = M$. Nodes can be labeled as generator machines (supply energy to the grid) or consumer machines (demand energy from the grid), thus $\vartheta = \vartheta_g \cup \vartheta_c$, being ϑ_g the set of generators and ϑ_c the set of consumers.

Let the dynamical state of each machine be represented by its phase angle ϕ_j and its phase velocity $\frac{d\phi_j}{dt} = \dot{\phi}_j$, $j \in \vartheta$. Under an appropriate operation of the power grid, it is expected that every machine will be rotating at some reference frequency Ω (which by convention is either $2\pi \times 50$ Hz or $2\pi \times 60$ Hz), so let the phase deviation of the machine j against the reference angle Ωt be:

$$\theta_{j(t)} = \phi_{j(t)} - \Omega t \tag{2-8}$$

By applying the energy conservation law on each machine, the following equation for power balance is obtained:

$$P_j^m = P_j^d + P_j^a + P_j^t \tag{2-9}$$

Where:

P_j^m: The power generated or consumed by the machine.
P_j^d: The power dissipated by the machine.
P_j^a: The power stored by the machine.

P_j^t: The power transmitted from the j-th machine to the rest of the power grid.

By introducing a constant D_j as the damping torque related to the j-th synchronous machine, dissipated power due to viscous friction can be expressed as:

$$P_j^d = D_j \dot{\phi}_j^2 \tag{2-10}$$

On the other hand, the accumulated power in a rotating synchronous machine with a moment of inertia I_j is given by the change of its kinetic energy in time, thus we have:

$$P_j^a = \frac{I_j}{2} \frac{d\left(\dot{\phi}_j^2\right)}{dt} \tag{2-11}$$

Note that from Equation (2-8), $\dot{\phi}_j = \frac{d\phi_{j(t)}}{dt} = \Omega + \dot{\theta}_{j(t)}$; then going back to Equation (2-9), we get:

$$P_j^m = D_j \dot{\phi}_j^2 + \tfrac{I_j}{2} \tfrac{d\left(\dot{\phi}_j^2\right)}{dt} + P_j^t \tag{2-12}$$

$$P_j^m = D_j \left(\Omega + \dot{\theta}_{j(t)}\right)^2 + \tfrac{I_j}{2} \tfrac{d\left(\left(\Omega + \dot{\theta}_{j(t)}\right)^2\right)}{dt} + P_j^t \tag{2-13}$$

$$P_j^m = D_j \Omega^2 + 2 D_j \Omega \dot{\theta}_{j(t)} + \dot{\theta}_{j(t)}^2 + \tfrac{I_j}{2} \left[2 \left(\Omega + \dot{\theta}_{j(t)}\right) \left(\dot{\Omega} + \ddot{\theta}_{j(t)}\right)\right] + P_j^t \tag{2-14}$$

Under controlled operation of the power grid, the deviations of the phase velocity are expected to be small compared to the reference frequency, that is, $\Omega \gg \left|\dot{\theta}_{j(t)}\right|$. With this assumption and remembering that Ω is a fixed value (that is $\dot{\Omega} = \frac{d\Omega}{dt} = 0$), Equation (2-14) takes the form:

$$P_j^m = D_j \Omega^2 + 2 D_j \Omega \dot{\theta}_{j(t)} + I_j \Omega \ddot{\theta}_{j(t)} + P_j^t \tag{2-15}$$

$$I_j \Omega \ddot{\theta}_{j(t)} = P_j^m - D_j \Omega^2 - 2 D_j \Omega \dot{\theta}_{j(t)} - P_j^t \tag{2-16}$$

which is basically the so-called *swing equation*, a frequently used model in the field of power systems engineering to test angular stability of synchronous machines [65, 9]. Other extended models also include the voltage dynamics among other phenomena which yield to more complex differential-algebraic models, but those are out of the scope of this work [66].

To derive an appropriate expression for the transmitted power term P_j^t, some fundamental circuit theory is required and thus introduced in the next section.

2.3.1. Electrical Power Transmission

A power grid is a large alternating current (AC) circuit where voltage V and current I signals vary in time with some phases ϕ_v and ϕ_i and some fixed frequency ω. This can be summed up in the complex representation:

$$V_{(t)} = \hat{V} e^{i(\omega t + \phi_v)} \tag{2-17}$$

$$I_{(t)} = \hat{I} e^{i(\omega t + \phi_i)} \tag{2-18}$$

Being $\hat{V}$ and $\hat{I}$ the amplitude of voltage and current respectively. It can be shown that the complex power, also known as apparent power is given by:

$$S = \bar{V}\bar{I}^* \tag{2-19}$$

Where $\bar{V}$ is the root mean square (RMS) value of V, that is $\bar{V} = \frac{\hat{V}}{\sqrt{2}}$ and similarly $\bar{I}^*$ means the RMS value of the complex conjugate of I. By taking the real and imaginary parts of S, active power P and reactive power Q are defined respectively as:

$$P = \Re\{S\} = \frac{\hat{V}\hat{I}}{2}\cos(\phi_v - \phi_i) \tag{2-20}$$

$$Q = \Im\{S\} = \frac{\hat{V}\hat{I}}{2}\sin(\phi_v - \phi_i) \tag{2-21}$$

Consider the simplest circuit possible, where two nodes with voltages V_i and V_j, respectively, are connected by an impedance Z_{ij} through which a current I_{ij} flows. Applying Ohm's law, this current can be expressed as:

$$I_{ij} = \frac{V_i - V_j}{Z_{ij}} \tag{2-22}$$

In a power grid it is expected that the voltage amplitude of every node (generators and consumers) is approximately the same, that is $\hat{V}_i = \hat{V}_j = \hat{V}$, then:

$$I_{ij} = \frac{\hat{V}e^{i(\omega t + \phi_i)} - \hat{V}e^{i(\omega t + \phi_j)}}{Z_{ij}} = \hat{V}e^{i\omega t}\left[\frac{e^{i\phi_i} - e^{i\phi_j}}{Z_{ij}}\right] \tag{2-23}$$

Note that, the voltage dynamics are being ignored when taking V as a constant around the whole network; a more detailed model has to include the effects of such dynamics in a set of differential-algebraic equations, but that is out of the scope of this work.

Impedance Z_{ij} can be expressed as a combination of a resistance R_{ij} and a reactance X_{ij} as follows:

$$Z_{ij} = R_{ij} + iX_{ij} \tag{2-24}$$

For simplicity, admittance Y_{ij} is introduced as the inverse of impedance, that is:

$$Y_{ij} \equiv \frac{1}{Z_{ij}} = G_{ij} + iB_{ij} = |Y_{ij}|\, e^{i\alpha_{ij}} \tag{2-25}$$

$$G_{ij} = \frac{R_{ij}}{R_{ij}^2 + X_{ij}^2} \tag{2-26}$$

$$B_{ij} = \frac{-X_{ij}}{R_{ij}^2 + X_{ij}^2} \tag{2-27}$$

$$\alpha_{ij} = \arctan\left(\frac{B_{ij}}{G_{ij}}\right) = \arctan\left(\frac{-X_{ij}}{R_{ij}}\right) \tag{2-28}$$

Equation (2-23) is then turned into:

$$I_{ij} = \hat{V}\,|Y_{ij}|\left(e^{i\phi_i} - e^{i\phi_j} + e^{i\alpha_{ij}}\right) e^{i\omega t} \tag{2-29}$$

Whose RMS value is simply:

$$\bar{I}_{ij} = \frac{\hat{V}\,|Y_{ij}|}{\sqrt{2}}\left(e^{i\phi_i} - e^{i\phi_j}\right) e^{i\alpha_{ij}} \tag{2-30}$$

The apparent power flowing through nodes i and j is then given by:

$$S_{ij} = \bar{V}_i \bar{I}_{ij}^* = \left[\frac{\hat{V}e^{i\phi_i}}{\sqrt{2}}\right]\left[\frac{\hat{V}|Y_{ij}|}{\sqrt{2}}\left(e^{-i(\phi_i+\alpha_{ij})} - e^{-i(\phi_j+\alpha_{ij})}\right)\right] \tag{2-31}$$

$$S_{ij} = \frac{\hat{V}^2|Y_{ij}|}{2}\left(e^{-i\alpha_{ij}} - e^{i(\phi_i-\phi_j-\alpha_{ij})}\right) \tag{2-32}$$

By taking the real and imaginary parts of S we have:

$$P = \Re\{S\} = \frac{\hat{V}^2|Y_{ij}|}{2}\left(\cos\alpha_{ij} - \cos(\phi_i - \phi_j - \alpha_{ij})\right) \tag{2-33}$$

$$Q = \Im\{S\} = -\frac{\hat{V}^2|Y_{ij}|}{2}\left(\sin\alpha_{ij} - \sin(\phi_i - \phi_j - \alpha_{ij})\right) \tag{2-34}$$

In the following, reactive power Q will be neglected and only active power transfer P will be considered [19], then by defining a new angle γ_{ij} as:

$$\gamma_{ij} \equiv \alpha_{ij} - \frac{\pi}{2} \tag{2-35}$$

Equation (2-33) turns into:

$$P = \frac{\hat{V}^2 \left|Y_{ij}\right|}{2} \left(\cos \alpha_{ij} - \sin(\phi_i - \phi_j - \gamma_{ij})\right) \tag{2-36}$$

Note that from Equation (2-25) we have $\Re\{Y_{ij}\} = G_{ij} = |Y_{ij}| \cos \alpha_{ij}$, so the electrical active power transfered from a node i to a node j is finally expressed as:

$$P = \frac{\hat{V}^2 G_{ij}}{2} - \frac{\hat{V}^2 \left|Y_{ij}\right|}{2} \sin(\phi_i - \phi_j - \gamma_{ij}) \tag{2-37}$$

2.3.2. From Power Grids to the Kuramoto Model

The equation of motion derived in (2-16) is now completed by including the transmitted power (2-37), so by accounting for every existing link (i, j) in the network, and using the fact that the phase difference $\phi_i - \phi_j = \theta_i - \theta_j$, the equation of motion for the j-th machine is transformed into:

$$I_j \Omega \ddot{\theta}_{j(t)} = P_j^m - D_j \Omega^2 - 2D_j \Omega \dot{\theta}_{j(t)} - \sum_{i \neq j}^{N} \left[\frac{\hat{V}^2 G_{ij}}{2} - \frac{\hat{V}^2 |Y_{ij}|}{2} \sin(\theta_j - \theta_i - \gamma_{ji}) \right] \tag{2-38}$$

$$\ddot{\theta}_{j(t)} = \left(\frac{2P_j^m - 2D_j \Omega^2 - \hat{V}^2 \sum\limits_{i \neq j}^{N} G_{ij}}{2I_j \Omega} \right) - \left(\frac{2D_j \Omega}{I_j \Omega} \right) \dot{\theta}_{j(t)} + \frac{\hat{V}^2}{2I_j \Omega} \sum_{i \neq j}^{N} |Y_{ij}| \sin(\theta_j - \theta_i - \gamma_{ji}) \tag{2-39}$$

Note that, by the definition of matrix Y, it follows that $G_{jj} = \sum\limits_{i \neq j}^{N} G_{ij}$, so we finally write:

$$\ddot{\theta}_{j(t)} = \left(\frac{2P_j^m - 2D_j \Omega^2 - \hat{V}^2 G_{jj}}{2I_j \Omega} \right) - \left(\frac{2D_j \Omega}{I_j \Omega} \right) \dot{\theta}_{j(t)} + \frac{\hat{V}^2}{2I_j \Omega} \sum_{i \neq j}^{N} |Y_{ij}| \sin(\theta_j - \theta_i - \gamma_{ji}) \tag{2-40}$$

This equation is simplified by defining new parameters P_j, α_j and K_{ji} as:

$$P_j \equiv \left(\frac{2P_j^m - 2D_j \Omega^2 - \hat{V}^2 G_{jj}}{2I_j \Omega} \right) \tag{2-41}$$

$$\alpha_j \equiv \left(\frac{2D_j \Omega}{I_j \Omega} \right) \tag{2-42}$$

$$K_{ji} \equiv \frac{\hat{V}^2 |Y_{ij}|}{2I_j \Omega} \tag{2-43}$$

Here K_{ji} are the elements of the connectivity matrix K, which gives information about the topology of the power grid composed of N rotating machines.

$$\ddot{\theta}_{j(t)} = P_j - \alpha_j \dot{\theta}_{j(t)} + \sum_{i}^{N} K_{ji} \sin(\theta_{i(t)} - \theta_{j(t)} - \gamma_{ji}) \tag{2-44}$$

In real-world power grids usually the resistance in the transmission lines can be neglected, which is a common assumption in power systems engineering. This assumption can be introduced in Equation (2-44) to derive a no-loss model by setting to zero the real part of the complex admittance matrix Y, that is, $G_{ij} = 0$ for all i and j. This also implies that $\alpha_{ij} = \frac{\pi}{2}$ and therefore $\gamma_{ij} = 0$. We get then:

$$\ddot{\theta}_{j(t)} = P_j - \alpha_j \dot{\theta}_{j(t)} + \sum_{i}^{N} K_{ji} \sin(\theta_{i(t)} - \theta_{j(t)}) \tag{2-45}$$

with:

$$P_j \equiv \left(\frac{2P_j^m - 2D_j\Omega^2}{2I_j\Omega} \right) \tag{2-46}$$

It can be shown that for the dynamical system described in Equation (2-44) to reach a steady state $\ddot{\theta} = \dot{\theta} = 0$, the following power balance condition has to be satisfied:

$$\sum_{i}^{N} P_i = 0 \tag{2-47}$$

That is to say, the power supplied to the network by the generators must be equal to the power consumed by the loads [23].

Interestingly, Equation (2-44) is equivalent to the celebrated second-order *Kuramoto model*, which has been widely used to describe the collective dynamics in a variety of physics, biology, engineering and social sciences applications that involve interacting oscillatory agents [67, 68, 69, 21]. This model was originally proposed in 1975, as a way to model the behavior of an infinite population of coupled non-linear oscillators through the set of first-order differential equations:

$$\dot{\theta}_{j(t)} = \omega_j + K \sum_{i}^{N} a_{ji} \sin(\theta_{i(t)} - \theta_{j(t)}) \tag{2-48}$$

Where ω_j is called the *natural frequency* of the j-th agent in the ensemble and a_{ji} are the elements of the adjacency matrix A.

Note that the original Kuramoto model (2-48) only included first-order dynamics; the second derivative of the phase angle was later added to account for inertia in some specific study cases, leading to model (2-45). Furthermore, Equation (2-48) impossed the assumption of an homogeneous coupling strength K for every pair of connected oscillators.

Equation (2-48) was found to exhibit some interesting and very intuitive behavior: when the interaction between oscillators is weak, or in other words, when the coupling constant K is small, each oscillator tends to rotate at some phase velocity close to its natural frequency ω_j; conversely, when interactions are strong, that is to say, there is a large K value, all oscillators in the ensemble will tend to rotate at the same frequency ω_s and thus *synchronization* of the ensemble is achieved. This means that there exists a transition from a disordered to an ordered phase in the system when the coupling strength K is increased beyond a certain critical coupling value K_c [70]. As will be explained later, this phase transition also occurs in the more general, second-order model (2-45).

Both versions of the Kuramoto model have been widely studied through theoretical developments, like the mean-field theory [21, 25, 70, 71], as well as through intensive numerical simulations [24, 35, 72, 73, 74] and a large variety of phenomena have been discovered in both regimes.

In the framework of the Kuramoto model, it has been proposed that the loss of synchrony in the components of a power grid, even locally, may cause a partial malfunctioning, cascading failures and even the total blackout of the transmission network [19, 23, 75, 8, 9, 10], thus, in the following, this document will concentrate in the study of synchronization in the model described by Equation (2-45).

2.4. Random Growth Model for Power Grids

When the applicability of the Kuramoto model in the analysis of power systems is considered, it is important to have realistic example cases that can be used to test the theoretical approaches [76, 77]. Having that idea in mind, this section describes the algorithm proposed in [2] which allows generating complex networks that incorporate a spatial embedding (accounts for the geographic position of nodes) and that have similar structural properties to those found in real-world power grids.

For this algorithm, a redundancy cost function that will be subject to optimization has to be defined as:

$$f_{(i,j,G)} = \frac{(d_G(i,j)+1)^r}{d_S(x_i,x_j)} \tag{2-49}$$

where $d_G(i,j)$ is the length of the shortest path between nodes i and j in the graph G, $d_S(x_i,x_j)$ is the spatial distance (Euclidean distance) between the nodes positions x_i and x_j, and r is a parameter that controls the cost-vs-redundancy trade-off, that is to say, how much should the optimizer care about the spatial distance and the structural distance between a pair of nodes.

The algorithm requires the following input parameters:

- N_0: An initial amount of nodes, $N_0 \geq 1$.
- N: Final amount of nodes that the network will have $N \geq N_0$.
- $x = \{x_1, x_2, ..., x_N\}$: Geographical location of the initial nodes.
- p, q: Probabilities of constructing additional redundancy links in the network, such that $0 \leq p, q \leq 1$.
- s: Probability of splitting an existing line.
- r: Cost-vs-redundancy trade-off parameter for Equation (2-49).

The construction algorithm is developed through two phases: initialization and growth, which are performed as follows:

2.4.1. Initialization

1. Initialize a minimum spanning tree for the initial N_0 nodes such that it optimizes the edges that have to be built between them based on the minimum Euclidean distance $d_S(x_i,x_j)$ (refer to Figure **2-1**(a)). A minimum spanning tree refers to a graph that joins all the nodes without including any cycle and with the minimum total edge weight possible (in this construction stage, the weight of an edge is given by the Euclidean distance between the pair of nodes it connects).
2. Let $m = \lfloor N_0(1-s)(p+q) \rfloor$. For each $h = \{1, 2, ..., m\}$ find the pair of nodes (i,j) that are not yet linked and for which $f_{(i,j,G)}$ is maximal and connect them (as illustration, observe Figure **2-1**(b)).

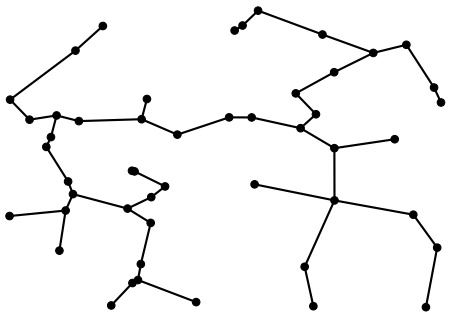

(a) Minimum spanning tree initialization.

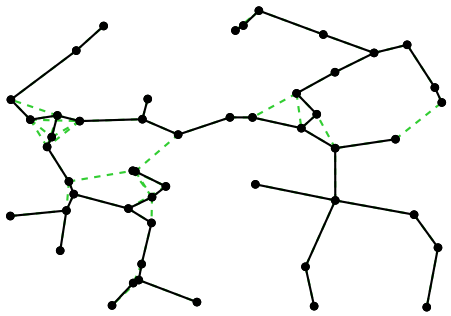

(b) Addition of redundant links based on the maximum $f_{(i,j,G)}$.

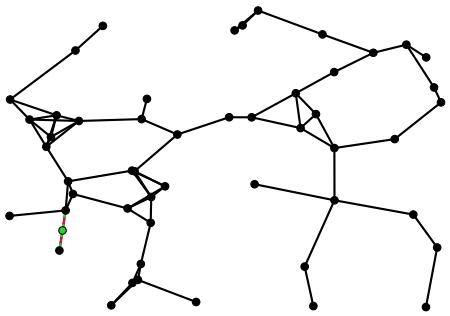

(c) Line splitting and node addition.

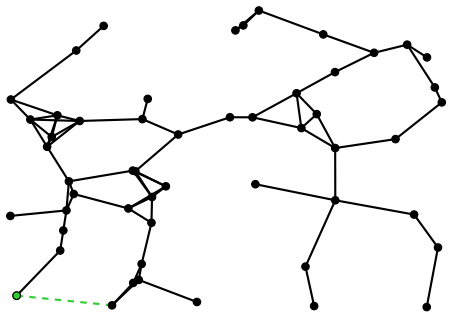

(d) Adding a link between the pair based on minimum $d_S(x_i, x_j)$.

Figure 2-1.: Some steps of the synthetic power grid generation algorithm. Green edges and nodes represent elements to be added, while red edges represent removed lines.

2.4.2. Growth

1. For each $h = \{1, 2, ..., N - N_0\}$ do:

   a) Add a new node h to the graph.

   b) Generate a random number ζ_1. If $\zeta_1 \leq 1 - s$ then:

   - Set the position of the new node x_h.
   - Add a link between the new node h and the closest node j geographically, that is, the node j for which $d_S(x_h, x_j)$ is minimal (see for instance, Figure **2-1**(d)).
   - Generate a random number ζ_2, if $\zeta_2 < p$ add a link between the new node h and some node l for which $f_{(h,l,G)}$ is maximal.
   - Generate a random number ζ_3, if $\zeta_3 < q$ draw a node h' from the network uniformly at random. Then find the node l' that is not yet linked to h' and for which$f_{(h,l,G)}$ is maximal and connect them.

   c) Otherwise (if $\zeta_1 > 1-s$), select an edge (i, j) of the network uniformly at random. The new geographic location of node h will be given by $x_h = {}^{(x_i+x_j)}/_2$, so the edge (i, j) is removed from the graph and then the edges (i, h) and (h, j) are added (for reference, observe Figure **2-1**(c)).

For illustration, Figure **2-2** shows some random networks generated with this algorithm for different structural parameters, together with the resulting degree distribution.

An interesting study that has to be considered is the one reported in [36], where this random growth model was used to test the dynamical stability and resilience to structural cascading failures for networks with a varying value of the redundancy parameter r. It was shown that for the constructed power grids, low values of r represent high (low) local (global) redundancy, measured in terms of transitivity (which is related to the clustering coefficient); while high values of this parameter represent a low (high) local (global) redundancy, as measured by the second-smallest eigenvalue of the Laplacian matrix, known as the algebraic connectivity. On these terms, it was concluded that a highly locally redundant grid is more robust to cascading failures, while a highly globally redundant grid possesses a lower proportion of critical nodes (nodes with poor dynamical stability). This implies that a trade-off has to be considered in the design of power grids between local and global connectivity redundancy.

This algorithm will be used in the next chapter to build test cases for resilience measures.

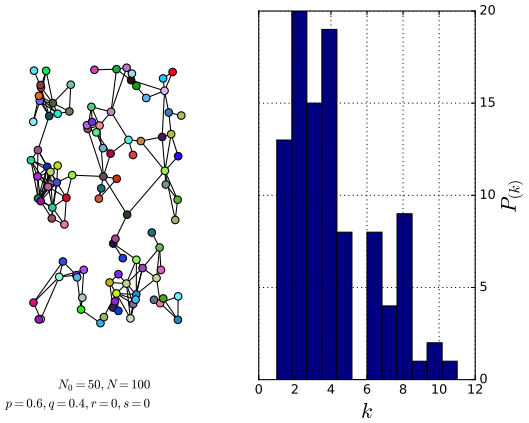

(a) $p = 0.6$, $q = 0.4$, $r = 0$, $s = 0$.

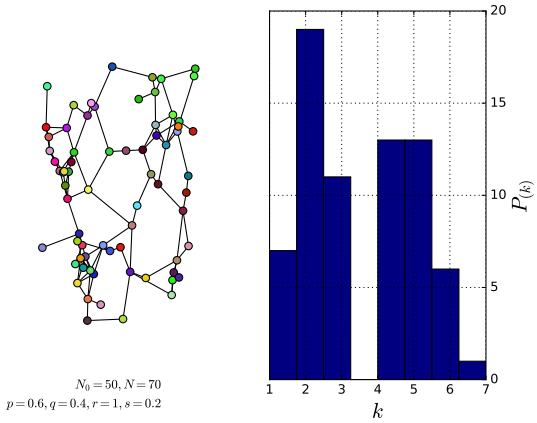

(b) $p = 0.6$, $q = 0.4$, $r = 1$, $s = 0.2$.

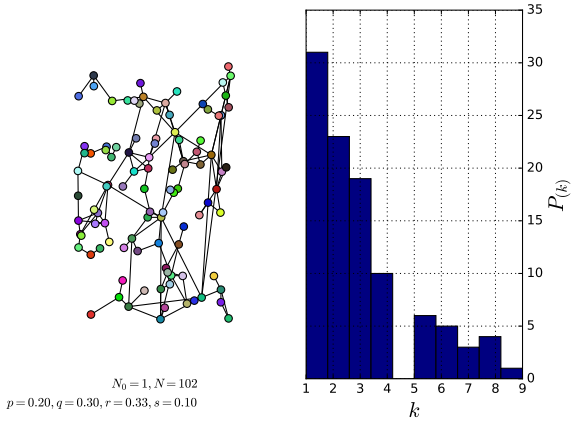

(c) $p = 0.2$, $q = 0.3$, $r = 0.33$, $s = 0.1$.

Figure 2-2.: Some spatially embedded power grids generated with the algorithm proposed in [2]. The histograms show the degree distribution of the network.

It has to be mentioned that this and any other graph building algorithm is just an ideal approximation of the real experiment, where the construction of power stations and transmission lines is not performed at random; it goes through a carefully planned process that takes into consideration geography of the region, the implementation cost, the relative location of cities and power sources (coal, oil or water resources), among other factors [78].

2.5. Tree-like Classification of Nodes

While studying the influence of topology of the network in the non-linear stability and survivability of the coupled oscillators, it was found in [3] that interesting patterns can be

spotted if nodes are classified according to their location in tree-shaped arrangements. Five categories were defined: *bulk nodes*, *roots*, *inner tree nodes*, *proper leaves*, *sparse sprouts* and *dense sprouts*. To explain each category, some definitions are required:

- A graph $G(\vartheta, \varepsilon)$ is called a *tree* if it is connected and has no cycles. A *tree-shaped part* $T'(\vartheta', \varepsilon')$ is a subgraph of G which is a tree, has the maximum possible size and has exactly one node $r \in \vartheta'$ that has at least one neighbour in the rest of the graph $G_2 = G - T'$. Node r is called the root of T' and has a degree $\hat{d}_r \geq 3$.
- Any node in G that does not belong to a tree-shaped part, is called a *bulk node*.
- Any node $l \in T'$ that is not a root but has exactly 1 neighbour, that is $\hat{d}_l = 1$, is called a *leaf*. However if $\hat{d}_l > 1$, node l is said to be an *inner tree node*.
- The *depth* of a node i that belongs to a tree-shaped part $i \in T'$, denoted by $\delta(i)$, is the shortest path from node i to the root of T'. Also, the *height* of such node $H(i)$ is the length of the longest path from i to a leaf of T'.
- If some leaf l has a depth $\delta(l) = 1$, it is named a *sprout*. Conversely, if $\delta(l) > 1$, it is called a *proper leaf*.
- Finally, a sprout s can be given the name of *sparse sprouts*, when the average degree of the neighbours of s is lower than 6, and *dense sprouts* otherwise.

Figure **2-3** shows an example of said classification in a randomly generated network after reproducing the classification algorithm described in the mentioned paper.

By using this classification, [3] discovered some novel asymptotic state where a machine located in a dense sprout oscillates at a velocity different to its natural frequency while the rest of the network is synchronized. Other important insights were extracted from this work, for instance, inner tree nodes should be avoided since they usually have low non-linear stability (as also confirmed by [30]). Furthermore, nodes with a high degree should also be avoided, since they have the worst survivability and hence poor transient stability. The authors also recommend leading the power grid design towards more regular network structures, since it has been shown in other relevant studies that homogeneous topologies are usually easier to synchronize than tree-shaped ones [79, 80].

2.6. Percolation

Percolation is a theory that deduces general macroscopic properties of an ensemble of interconnected elements in terms of the statistical description of its composition, the characteristics of the individual elements, and the topological arrangements of said elements. In this

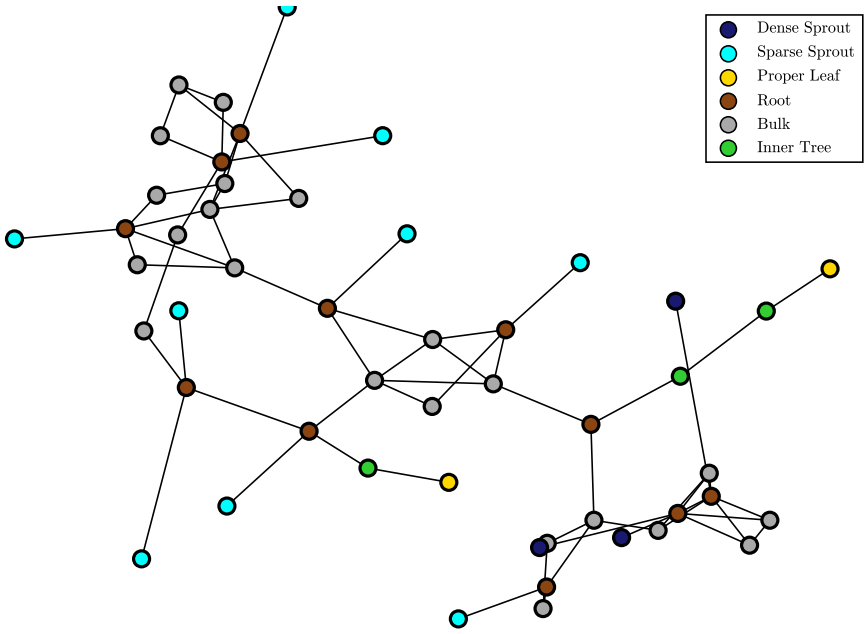

Figure 2-3.: Tree-like classification of nodes proposed in [3].

framework, a basic characteristic ensemble is usually defined and then topological variations are slowly applied in order to study their influence on those macroscopic properties of interest.

Two varieties of percolation are studied this work, those are bond percolation and site percolation. Bond percolation refers to cases when interactions between the elements are changed, removed or included, for instance, it aims to solve questions like: what is the maximum fraction of links, in average, that can be removed in a network before it breaks into multiple unconnected clusters?. Similarly, site percolation deals with problems where the elements are changed, removed or added; for instance: what minimum concentration of metallic atoms in an initially insulating medium have to be added in order to have electrical conductivity? [81].

In this work, as will be described in Chapter 4, percolation problems will be formulated, where nodes or edges in the power grid will be removed sequentially, aiming to represent element failures.

3. Synchronization Dynamics

3.1. Abstract

This chapter introduces the synchronization phenomenon, as well as some important theoretical tools that have been developed in the last years to analyse collective behavior in populations of interacting oscillators.

3.2. Synchronization of Coupled Oscillators

Given the second-order Kuramoto model (2-45), the dynamical system is said to be in a *phase synchronized* state if $\theta_{i(t)} = \theta_{j(t)}$, $\forall i, j \in \vartheta$, and in a *frequency synchronized* state if $\dot{\theta}_{i(t)} = \dot{\theta}_{j(t)} = \omega_s$, $\forall i, j \in \vartheta$, where $\omega_s = 0$ given the co-rotating reference frame Ωt used (as mentioned in Equation (2-8)) [8].

In addition, a solution for the system (2-45) will be said to have *cohesive phases* if $|\theta_i - \theta_j| < \gamma$, $\forall (i, j) \in \varepsilon$, with $0 \leq \gamma < \pi/2$; that is, for any pair of connected oscillators, the phase difference between them is no larger than $\pi/2$ [8].

As a way to measure the phase synchronization level in an ensemble of N interacting oscillators, Yoshiki Kuramoto proposed a complex valued order parameter given by:

$$re^{i\Psi_{(t)}} = \frac{1}{N}\sum_{i}^{N} e^{i\theta_{i(t)}} \tag{3-1}$$

Here, $\Psi_{(t)}$ is the average phase of the oscillators at time t. If all phases θ_i are identical, the magnitude of the order parameter is $r_{(t)} = 1$. On the other hand, if they are equally distributed around the unit circle the system is said to be desynchronized and $r_{(t)} = 0$. Intermediate values of r correspond to partially synchronized states [22]. Additionally, in the case of power grids in which Equation (2-47) holds, when the system is synchronized, the real part of the order parameter $\mathbb{R}[r] \approx 1$, while it oscillates around zero otherwise. While the dependence of the order parameter with time is useful in transient analysis, we

will focus on the steady state behaviour, so we can define the average order parameter in steady state as [23]:

$$r_\infty = \lim_{t_1\to\infty}\left[\lim_{t_2\to\infty}\left(\frac{1}{t_2}\int_{t_1}^{t_1+t_2} r_{(t)}dt\right)\right] \tag{3-2}$$

Another measure of frequency synchronization in power grids is the squared average rotational speed $v^2_{(t)}$ defined as [23]:

$$v^2_{(t)} = \frac{1}{N}\sum_i^N \dot{\theta}^2_{i(t)} \tag{3-3}$$

and the associated steady state value of the speed v_∞:

$$v_\infty = \sqrt{\lim_{t_1\to\infty}\left[\lim_{t_2\to\infty}\left(\frac{1}{t_2}\int_{t_1}^{t_1+t_2} v^2_{(t)}dt\right)\right]} \tag{3-4}$$

3.3. Synchronization in a Simple System

Consider the simplest system composed of one generator and one consumer and let its dynamics be described by Equation (2-45). For this two-node system, it is more convenient to deduce the differential dynamics given by $\Delta\theta = \theta_2 - \theta_1$ and $\Delta\chi = \dot{\theta_2} - \dot{\theta_1}$, thus, from Equation (2-45), we get:

$$\begin{aligned} \Delta\dot{\theta} &= \Delta\chi \\ \Delta\dot{\chi} &= P_2 - P_1 - \alpha\Delta\chi - 2K\sin(\Delta\theta) \end{aligned} \tag{3-5}$$

For this system, two equilibrium points $E_1 = (\Delta\chi_1^*, \Delta\theta_1^*)$ and $E_2 = (\Delta\chi_2^*, \Delta\theta_2^*)$ can be calculated analytically by setting $\Delta\dot{\theta} = 0$ and $\Delta\dot{\chi} = 0$, yielding:

$$E_1 = \begin{bmatrix}\Delta\chi_1^* \\ \Delta\theta_1^*\end{bmatrix} = \begin{bmatrix}0 \\ \arcsin(\frac{P_2-P_1}{2K})\end{bmatrix} \tag{3-6}$$

$$E_2 = \begin{bmatrix}\Delta\chi_2^* \\ \Delta\theta_2^*\end{bmatrix} = \begin{bmatrix}0 \\ \pi - \arcsin(\frac{P_2-P_1}{2K})\end{bmatrix} \tag{3-7}$$

Clearly, E_1 and E_2 can only exist for $2K \geq P_2 - P_1$, and, in particular, when $2K = P_2 - P_1$, then $E_1 = E_2$ and it is a neutrally stable equilibrium. It can be proven, by extracting the eigenvalues of the Jacobian for the system (3-5), that in the case $2K > P_2 - P_1$, the first equilibrium E_1 has both eigenvalues with a negative real part, thus it is a locally stable equilibrium; while the second equilibrium E_2 is unstable. More precisely, it is a saddle point, with one eigenvalue with negative real part and another eigenvalue with positive real part.

This means that the equilibrium (and by extension, a normal operation o the power grid) can only exist for $K > {}^{(P_2-P_1)}/_2$. This can be tested by setting the parameters to $P_1 = 1$, $P_2 = -1$ and $\alpha = 1$ and studying the effect of varying the coupling constant K.

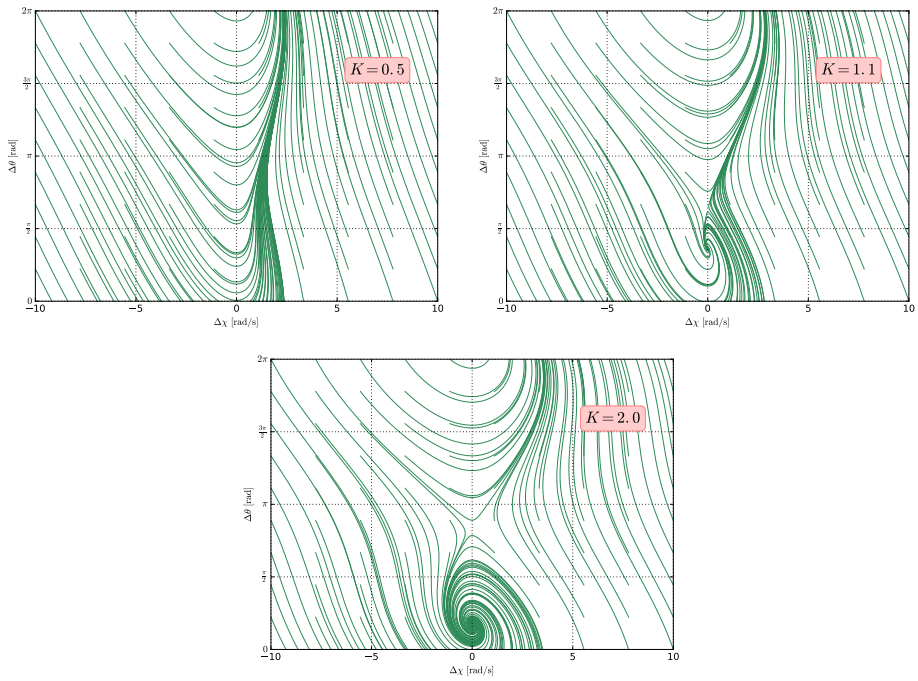

Figure 3-1.: Phase plane for a system of one generator and one consumer for different values of coupling strength (a) $K = 0.5$, (b) $K = 1.1$ and (c) $K = 2.0$.

Figure **3-1** shows the phase plane of the second order differential phase dynamics (3-5). When the coupling is not strong enough, as in the case of $K = 0.5$, there exists a globally stable limit cycle, related to an undesirable continuously varying rotating frequency on the system; synchronization can never be achieved.

If the coupling strength is increased to $K = 1.1$, a locally stable equilibrium point appears at the location given by (3-6), that is $E_1 \approx (0, 1.14)$ while a saddle point appears at the location (3-6), which is roughly $E_2 \approx (0, 2)$. E_1 and E_2 also coexist with the locally stable limit cycle that leads to the power outage of the network. Note that reaching exactly E_2 in a

practical experiment is impossible since any small disturbance around this point would lead the dynamical system to either E_1 or the undesired limit cycle, thus in the following, the desired frequency synchronized state would be the stable equilibrium E_1.

When K is further increased to 2.0, the limit cycle disappears and the locally stable fixed point E_1 becomes globally stable, meaning that for any given initial condition (except of course the impractical saddle point E_2), the system itself can recover the synchrony after some transient time. For this particular value of K, the locations of the equilibrium points are $E_1 \approx (0, 0.52)$ and $E_2 \approx (0, 2.62)$.

Although this is the simplest network case, this example gives important insights about the power grid model (2-45) that can be extended to a large-N situation; loosely speaking, it reveals that to guarantee a correct functioning on a power grid, transmission lines need to be "strong enough", such that they allow the existence of the frequency synchronized state.

The dynamical system described by Figure **3-1** is said to go through two *bifurcation* points, in other words, the qualitative behaviour of the solutions changes when a parameter (in this case K) is modified. The first bifurcation occurs in the transition from panel (a) to panel (b) of the same Figure and the locally stable fixed point appears. In [82], after some algebraic treatment of the second-order Kuramoto model, and assuming $\alpha_j = \alpha$, $\forall j$, it was found that the K_{fp} value for which this first bifurcation occurs can be computed as:

$$K_{fp} = \max_i \left\{ \frac{|\alpha\omega_s - P_i|}{\hat{d}_i} \right\} \tag{3-8}$$

where $\hat{d}_i$ is the node degree and ω_s is the synchronization frequency, which, as mentioned before, can be assumed to be $\omega_s = 0$ [22], therefore (3-9) turns into:

$$K_{fp} = \max_i \left\{ \frac{|P_i|}{\hat{d}_i} \right\} \tag{3-9}$$

It means that for any $K < K_{fp}$, a synchronous state does not exist in the Kuramoto model. For $K \geq K_{fp}$, the synchronization manifold exists but is not necessarily globally stable.

3.4. Synchronization Depends on the Network Topology

It turns out that the transition from the disordered state (where each agent in the network oscillates at its own frequency) to a fully synchronized state depends in a non-trivial way on the topology of the complex network. To illustrate that, as well as to motivate further

discussion, Figure **3-2** reproduces the results from [23], where it is shown that the transition profile of the system changes drastically when a random, small-world or quasi-regular network arrangement is considered.

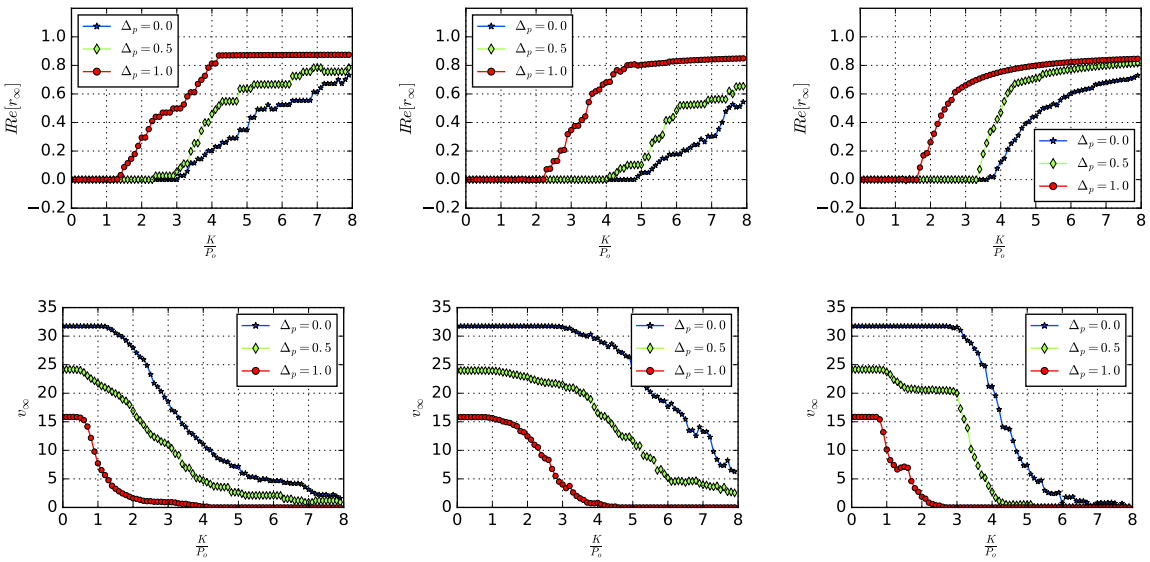

Figure 3-2.: Effect of varying coupling strength K in synchronization for different network topologies. Top row: real part of the order parameter in steady state $\mathbb{R}[r_\infty]$; bottom row: average speed in steady state v_∞. These results were averaged over 30 randomly initialized networks. $N = 120$, $P_{bg} = 10$, $P_{sg} = 2.5$ and $\alpha = 0.1$.

Note that, although these correspond to networks of roughly 120 nodes connected in completely different fashions, the general behaviour seen in the previous section for the two-node case, is conserved; increasing the relationship of K/P causes the averaged steady state speed v_∞ to drop to zero and the real part of the order parameter in steady state $\mathbb{R}[r_\infty]$ to rise from zero to a positive value, leading thus to a synchronous state after surpassing some unknown critical coupling K_c.

This study defines a parameter Δ_p to describe the proportion of the power that is generated by small power generators which produce just $1/4$ of the power supplied by any other (large) power generator, over the complete generated power, in other words:

$$\Delta_p = \frac{P_{sg}}{P_{bg} + P_{sg}} \tag{3-10}$$

where P_{sg} is the total power supplied by small generators while P_{bg} is the one generated by large power plants. As seen in Figure **3-2**, the critical coupling at which synchronization begins can change significantly when the rate of distributed power Δ_p is increased, that is,

when high-power generators are replaced by multiple low-power generators that satisfy the same demand. An interesting takeaway from this Figure is that a more distributed power generation (that is, a higher Δ_p), causes in general an easier synchronization of the complete network, as it requires a lower coupling strength in the transmission lines to reach the equilibrium point.

For further details about these simulations, the reader is encouraged to review the complete paper [23].

3.5. An Estimation for K_c

As discussed in the previous section, the topology of the complex network where the oscillators are arranged in, can significantly change the critical coupling K_c required for the system to drive itself to the frequency synchronized state. Consider the Kuramoto model with a simplified notation:

$$\ddot{\theta}_{j(t)} = P_j - \alpha_j \dot{\theta}_{j(t)} + k \sum_{i}^{N} a_{ji} \sin(\theta_{i(t)} - \theta_{j(t)}) \tag{3-11}$$

where, as explained in the previous chapter, the elements of the adjacency matrix are $a_{ji} \geq 0$ and k is the maximum power capacity of the transmission lines. In [8], by applying a linear approximation of the system (3-11) around the equilibrium point, an approximation for K_c was found, such that if $k \geq K_c$, the model (3-11) has a unique and stable solution with synchronized frequencies and cohesive phases.

Following the procedure in [8], it can be proven that, by applying a small-angle approximation to the model (3-11), the equilibrium phases $\theta^* \in \mathbb{R}^N$ can be estimated as:

$$\theta^* = \frac{1}{k} L^{\dagger} P \tag{3-12}$$

where $L^{\dagger}$ is the pseudo-inverse of the Laplacian matrix of the graph. Let us then define the phase difference between any pair of connected oscillators by:

$$\Delta_\theta = B\theta^* = \frac{1}{k} B^T L^{\dagger} P \tag{3-13}$$

where B is the oriented incidence matrix. The exponentially stable fixed point from Equation (3-12) also satisfies, for some angle $\gamma \in [0, \pi/2)$, the following condition:

$$||\Delta_\theta||_\infty \leq \sin(\gamma) \tag{3-14}$$

where the infinity norm operator used $||\Delta_\theta||_\infty = \max_{(i,j)\in\varepsilon} |\theta_i - \theta_j|$, in other words, the largest phase difference between any pair of connected nodes in the network. Then, by imposing the phase cohesiveness condition described in section 3.2, the following expression is derived:

$$||\Delta_\theta||_\infty < 1 \tag{3-15}$$

By substituting the (3-13) into Equation (3-15), the last one can be rewritten to provide the sufficient condition for the critical coupling K_c such that frequency synchronization can exist:

$$K_c \approx ||B^T L^\dagger P||_\infty \tag{3-16}$$

The synchronization concepts described by now, allow us to study the linear stability of the system (2-45), but information about the non-linear stability is still missing and will be described in a following section.

3.6. Braess Paradox

After seeing how the synchronization in the Kuramoto model is enhanced when K is increased, it would be fairly intuitive to think that adding new transmission lines to a power grid would have the same effect. However, as explained in [83], that is not necessarily the case; it was proven that there could be some specific edges that, when added to the complex network, would cause an increase of the critical coupling K_c and thus undermine and even destroy the synchronized state. This phenomenon was related to the *Braess paradox*, initially reported for traffic networks, which is produced by geometric frustration induced over the power flow cycles formed in the grid. That is the reason why the authors also note that it was found to occur more frequently in square lattices. This study had a lot of impact in the analysis of the Kuramoto model and has some evident implications in the structural design of power grids [84, 85, 86, 87, 88].

3.7. Cyclic Power Grids

As the topology of power grids is a matter of paramount relevance in its stability, the work presented in articles like [89] and [29], regarding ring-like arrangements, have to be mentioned. Specifically, it was argued in [89] that the emergence of vortex power flows in power grids causes a zero-net power transfer from producers to consumers; all the power is dissipated ohmically. These vortex flows correspond to the situation when a closed-loop in a power

grid has a *winding number* $q_\alpha = \frac{1}{2\pi}\sum_{k=1}^{n_\alpha} |\theta_{k+1} - \theta_k| \neq 0$, or in other words, the complex voltage rotates in the complex plane as one goes around a loop with n_α nodes. It was also shown that, even if initially the power grid has cyclic parts with $q_\alpha = 0$, non-local structural changes, as suppressing a transmission line in another section of the network, could induce a different state with $q_\alpha \neq 0$ due to power redistributions. Furthermore, repairing said line does not guarantee that the grid recovers its $q_\alpha = 0$ state. In the field of electrical engineering, loop flows are a very well-known phenomenon and the design methodologies of power grids currently account for them and prevent them by installing FACTS [90].

Alternatively, in [29], the linear stability of cyclic power grids was analysed using the classic characterization through the eigenvalues of the Jacobian and the non-linear stability was estimated by measuring energy barriers as the difference between the potential energy in the stable equilibrium and its closest type-1 equilibrium (the equilibrium point for which only one unstable direction is detected in the eigenvalues framework). Through this analysis, it was found that adding small cycles to the network (typically less than 10 nodes) improves the stability of the synchronized state to random disturbances.

3.8. Basin Stability

Consider a multistable dynamical system that lives in the state space X and let $X^* \subset X$ be the set of desirable attracting states. The *basin of attraction* of X^*, noted by β, is defined as the set of all initial conditions $x_{(0)}$ that asymptotically converge to X^* [30]. For the purpose of this work, X^* will be the frequency synchronization manifold of the system (2-44), that is, the set of all frequency synchronized states as defined previously. It is worth mentioning that, in real-life electrical systems, the synchronization at frequencies far from the set point of 60 Hz or 50 Hz is not physically possible since most of the machines would fail and be severely damaged in such scenarios.

Similarly, the likelihood of a randomly perturbed trajectory to return back to β, known as the *basin stability* S_B, can be defined as [30, 31]:

$$S_B(\beta) = \int \Gamma_\beta(x)\rho(x)dx \tag{3-17}$$

where $\Gamma_\beta(x)$ is a function that indicates whether an state x belongs to the basin of attraction of X^* or not, that is

$$\Gamma_\beta(x) = \begin{cases} 1 & \forall x \in \beta \\ 0 & \forall x \notin \beta \end{cases} \tag{3-18}$$

The function $\rho_{(x)}$ is the density of states to which the system can be pushed by some non-local perturbation, such that $\int_X \rho_{(x)} dx = 1$. Note that under this definition, the basin stability is a number between 0 and 1, being $S_B = 0$ when the synchronous state is unstable and $S_B = 1$ when it is globally stable.

Monte Carlo simulations can be performed in order to estimate S_B by randomly sampling a sufficiently high number of disturbed states I_C (following a certain distribution $\rho_{(x)}$) from a representative subspace $\Pi \subset X$, and using them as the initial conditions for time-evolution simulations. For this work, $\rho_{(x)}$ is chosen as a uniform distribution in the restricted subspace Π, that is:

$$\rho(x) = \begin{cases} \frac{1}{|\Pi|} & \forall x \in \Pi \\ 0 & \forall x \notin \Pi \end{cases} \tag{3-19}$$

Finally, the amount F_C of simulated trajectories that are found to approach asymptotically to the attractor is assumed to be proportional to the volume of the basin of attraction (restricted to the subspace Π), thus S_B is approximated by $S_B \approx {}^{F_C}/_{I_C}$.

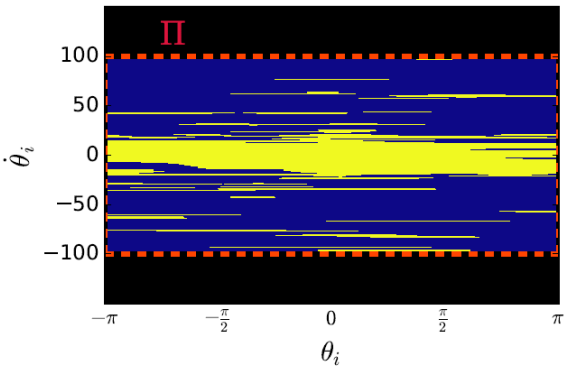

Figure 3-3.: Phase space of a randomly chosen node i when random disturbances are applied to θ_i or $\dot{\theta}_i$. Yellow zones are initial conditions that return to the frequency synchronized state, while the blue ones are out of the basin of attraction. The red dashed line denotes the subspace Π from which disturbances are chosen. This diagram was created by interpolating $I_C = 500$ random points.

To relate the concept of basin stability to the complex system (2-44), disturbances are applied at each node independently, in order define an indicator that provides information about the robustness of each oscillator to large perturbations applied to it, the so-called *single-node*

basin stability (SNBS) [31, 32], given by:

$$S_B^{(i)} = \frac{F_C}{I_C}, \quad i \in \vartheta \tag{3-20}$$

where the I_C initial conditions are drawn from perturbations applied to node i.

As an illustration, Figure **3-3** shows the phase diagram of some node i in a test network, subject to large disturbances; its SNBS is, loosely speaking, the proportion of the yellow area with respect to the area of Π.

As it is also expected, the basin stability strongly depends on the coupling strength K. To show that, consider a generator node connected through an infinite bus to a fixed reference frequency θ_g. The state of that system is then uniquely defined by the solution of the following second-order differential equation:

$$\ddot{\theta}_{(t)} = P - \alpha\dot{\theta}_{(t)} + K\sin(\theta_{(t)} - \theta_g) \tag{3-21}$$

Aiming to reproduce part of the results shown in [31], the parameters chosen are $\alpha = 0.1$, $P = 1$ and K is tested in the range $[0, 80]$. As observed in Figure **3-4**, the basin stability of this simple system increases as K is enhanced until the synchronized state is globally stable around $K \approx 64$. So it is understood that the green markers in the plot represent initial conditions that after some transient time converge to the synchronous state in the fixed point $(\theta, \dot{\theta}) = (\theta_s, 0)$, but, what happens with the red ones?. It turns out that they follow the same behaviour seen in Figure **3-1**(b) for intermediate values of K, there is a limit cycle coexisting with the fixed point somewhere in the phase plane. The location of said limit cycle can be estimated if it is guaranteed that ${}^{|P|}/_{\alpha^2} \gg 1$ and ${}^{|P|^2}/_{\alpha^2} \gg K$ [31], with the following expression:

$$\dot{\theta}_{lc(t)} \approx \frac{P}{\alpha} + \frac{\alpha K}{P}\cos\left(\frac{P}{\alpha}t\right) \tag{3-22}$$

So in Figure **3-4**(a), for instance, the attracting limit cycle lives approximately in the range $9.2 \leq \dot{\theta} \leq 10.8$.

In general, it would be expected that increasing K would raise the basin stability in a monotonic way (ignoring stochastic noise) as shown in Figure **3-4**(d), but it has been proven that it does not necessarily occur; it heavily depends in the topology of the complex network as well as in the power distribution of the nodes in a non-trivial way that remains unexplained [73, 88].

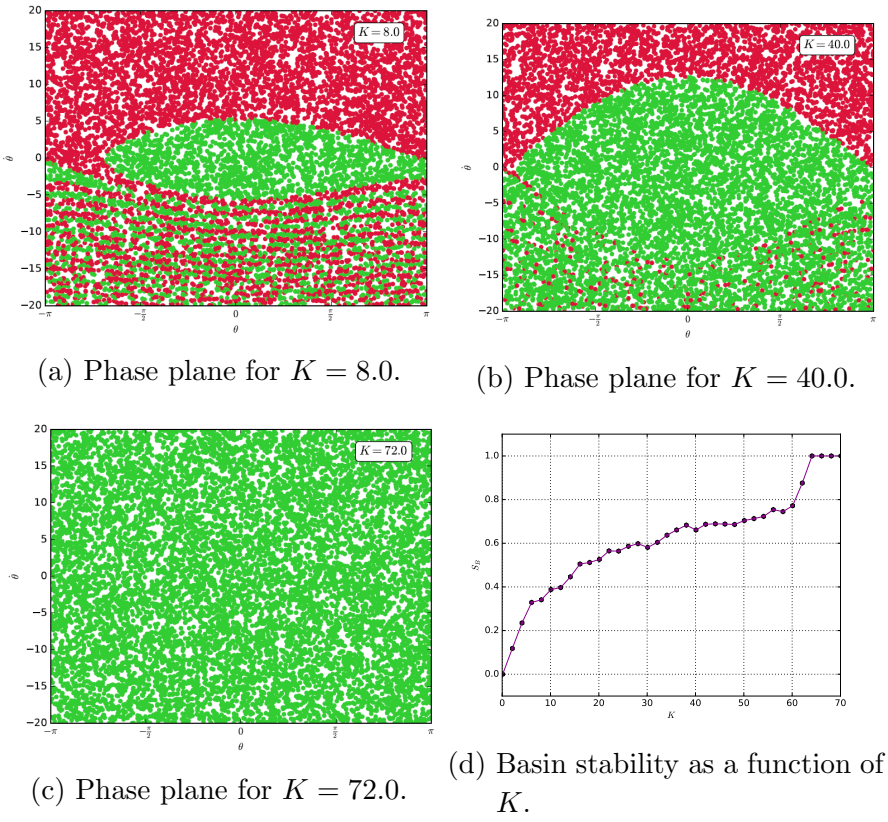

(a) Phase plane for $K = 8.0$.

(b) Phase plane for $K = 40.0$.

(c) Phase plane for $K = 72.0$.

(d) Basin stability as a function of K.

Figure 3-4.: Effect of varying coupling strength K in the non-linear stability of the infinite-bus model against random disturbances. Green dots represent initial conditions that belong to the basin of attraction, while red dots are the opposite.

The SNBS was later extended to the *multiple-node basin stability*, which considers disturbances applied in more than one node at the time, allowing to investigate underlying structure in the network, but increasing heavily the computational cost of the procedure [32].

It is also worth noting that the fine structure of the basin of attraction is not captured by this approach, and it could impose numerical problems on dynamical systems that posses either fractal basin boundaries or riddled or intermingled basins [91].

Another way to estimate the basin of attraction of this multi-dimensional system is by using the direct stability method of the Transient Energy Function (TEF), where a critical energy surface is calculated, such that if the system lies below that critical level after some fault, the system is stable; otherwise, it is unstable. This critical value of the energy is obtained by computing the Lyapunov-like function for the closest unstable equilibrium point (UEP), since it is assumed that the UEPs surround the stable synchronous state [27, 28, 92, 93]. This method, however, is not always applicable, since not all power systems possess an energy function [28], and finding all the UEPs could be a challenge [29].

Another interesting concept related to the non-linear stability of dynamical systems is the *survivability*, which was recently introduced in [94] and it is the fraction of perturbed initial conditions that evolve into trajectories that, during the desired analysed time window, never leave a desired region of the state space, making it especially useful to study the transient profile of the dynamical system. It was used successfully in [3] to discover interesting patterns in the Kuramoto model; in particular, a clear relationship between the survivability and the node degree was found, suggesting that a highly connected node is more prone to exhibit extreme transient behaviour for any kind of disturbance.

3.9. Recovery Time

To wrap up the discussion about stability against large perturbations, the *recovery time* defined in [33] is worth mentioning. Recovery time is a measure of the average time it takes for a randomly disturbed initial condition to settle back to the desired attractor (synchronization manifold in this particular case). It can be computed as follows:

$$t_r = \frac{\sum_{i=1}^{I_C}(t_l(x_d(i),\delta))}{I_C} \tag{3-23}$$

where $t_l(x_d(i),\delta)$ is the *settling time* for the trajectory starting at the initial condition $x_d(i)$, that is, the time spent by this trajectory to arrive sufficiently close to the desired attractor (such that its distance to the attractor is less than δ), and, as before I_C is the number of

initial conditions tested. As an illustration, Figure **3-5** shows the profile of the settling time in the phase plane for the infinite-bus model introduced in the previous section. A very intuitive idea can be confirmed from this picture: the trajectories that start on initial conditions closer to the equilibrium point converge faster to it than those located farther away. The recovery time is then, loosely speaking, the average of each coloured point in the figure.

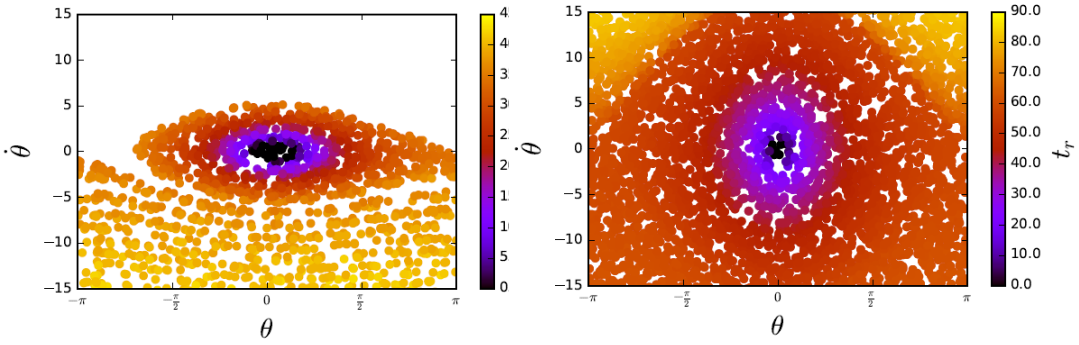

(a) Phase plane for $K = 8.0$.

(b) Phase plane for $K = 72.0$.

Figure 3-5.: Settling time for some random initial conditions sampled for the infinite-bus model. The white regions correspond to points that were not sampled. Recovery time would then be the average of every settling time in the plot.

Recovery time can be useful to identify slow nodes in the grid, that is to say, nodes that would take more time to reject a disturbance and return to its normal operation, which is crucial to diagnose since, taking a long time to recover, would cause the disturbance to spread over the whole network and possibly yield cascading failures and blackout. A drawback about using this measure is that it is not evident how to choose the initial conditions without previous and detailed knowledge of the basin of attraction.

4. Assessing Network Resilience

4.1. Abstract

This chapter proposes an algorithm to test the resilience of a power grid by applying continuous attacks that can be performed either at random or by focusing on the most vulnerable components of the network. Vulnerability is defined in terms of structural connectivity patterns of the nodes and the edges, as well as based on dynamical measures of the basin stability and phase difference between coupled oscillators.

4.2. Percolation-inspired Algorithm for Resilience Testing

In order to assess the resilience of a power grid, we propose a percolation-based algorithm. To do so, we will follow the capability of the network to maintain its functioning upon different node (nodal resilience) and edge (line resilience) removal rules. In particular, the algorithm that will be described below removes a node or an edge from the graph on each iteration by applying a *random attack*, where the element to be removed is chosen uniformly at random; or a *focal attack*, where the most vulnerable node or edge in the graph is removed first. Here, the most vulnerable node is the one with the smallest basin stability ($S_B^{(i)}$) or the highest degree centrality (d_k), clustering coefficient (c_k) or node betweenness centrality (b_k); while the most vulnerable edge is the one for which phase difference ($\Delta_\theta(i,j)$) or edge betweenness centrality (e_k) is the highest.

The percolation-based algorithm then proceeds as such:

1. Remove a node (edge) by applying a random or a focal attack. Note that in a focal attack, multiple nodes (edges) could share the same vulnerability level, in that case, the attacked node is chosen randomly among them.

2. Compute the existing disconnected clusters in the new graph.

3. For each cluster, check if it contains at least one generator node and one consumer node, if it does not, remove the whole cluster from the graph.

4. For each remaining cluster the power has to be compensated, so as a way to simulate a real-world power control (where the supplied power level is increased or reduced according to the demand of the consumers), the power of all generators in the cluster is modified uniformly such that Equation (2-47) remains true.

5. For each remaining cluster, check whether or not it is synchronizable, that is, its topology satisfies the synchronization condition that $K > K_c$, where K_c is computed by the approximation (3-16). If it does not, the whole cluster is removed from the graph.

6. Measure the needed observables and return to step 1 until the whole power grid has gone to blackout.

An important remark has to be done about the algorithm, regarding node removal under the focal attack methodology based on SNBS. Computing this vulnerability index is computationally expensive since it requires a huge amount of time-domain simulations in order to estimate reasonably well the Equation (3-20). Thus, in the following, only a few simulations in this regard are presented.

4.3. Test Case

To test the percolation algorithm just described, a set of synthetic power grids was generated with the random growth algorithm described in the section 2.4 and then those complex networks were subject to node or edge removal attacks. The parameters used for the growth model algorithm were chosen to match those used on [3], being: initial minimum spanning tree size $N_0 = 1$, redundancy line construction probabilities $p = 1/5$ and $q = 3/10$, redundancy-cost trade-off exponent $r = 1/3$, and line-splitting probability $s = 1/10$. The final size of the network is fixed to $N = 102$ and an equal amount of generators and consumers is placed to reduce heterogeneity in the samples (thus, $P_g = 1$, $\forall g \in \vartheta_g$ and $P_c = -1$, $\forall c \in \vartheta_c$). The dynamical model of the grid is rewritten as:

$$\ddot{\theta}_{j(t)} = P_j - \alpha_j \dot{\theta}_{j(t)} + k \sum_{i}^{N} a_{ji} \sin(\theta_{i(t)} - \theta_{j(t)}) \tag{4-1}$$

where $a_{ji} = \{0, 1\}$ are the elements of the adjacency matrix, the damping is set to $\alpha_j = 0.1$ and the maximum power transfer capacity is $k = 12.0$ (assuming an homogeneous coupling for every couple of connected oscillators). The order of magnitude for these parameters follows those found in the literature, where $\alpha_j = 0.1$ represents a decay time of 10 seconds for electromechanical disturbances [31].

4.3.1. Nodal Resilience

Figure **4-1**(a) shows the amount of nodes in the largest cluster of the network normalized by the original size N (called *giant component* of the graph and denoted by C) subject to node removal with focal and random attacking policies. For the SNBS case, only 10 simulations are considered due to the previously mentioned reason, while for each of the other cases, 500 simulations are performed.

Similarly, Figure **4-1**(b) presents the fraction of removed nodes after each iteration with respect to the original size (named *removed component* and denoted by $^{(N_{(0)}-N_{(I)})}/_{N_{(0)}}$), which allows to observe that the grid goes to complete blackout around the 40th removal iteration for the case of the focal attacking on either b_k and d_k, around the 60th iteration for the random and c_k attacking and with the largest standard deviation, between the 50th and 70th iteration for the S_B methodology.

By focusing the attacks on nodes with the highest b_k or d_k, the dimension of the giant component goes down drastically during the first elimination iterations and then it goes down with a lower rate, reaching total blackout around the 40th iteration. c_k on the other hand, produces a slower reduction of the graph size and a total blackout with the most iterations in average, pairing with the random scheme. This is related to the tree-like structure of the synthetic power grids; in this kind of topologies, the nodes with the higher degree and betweenness are located at the bulk regions of the graph, and their removal likely divides the giant component instantly into multiple smaller clusters, as also confirmed by the Figure **4-2**(a), where it is shown that these methodologies produce by far, the highest amount of operational clusters during the whole procedure.

Correspondingly, a node with a high clustering coefficient, by definition, implies that the neighbours that it is connected to, are also connected between them, hence, removing it is not going to divide the graph and generate new clusters. Eventually, after multiple node eliminations, redundant links between said neighbours will be suppressed and c_k will become uniform over the whole system. That is the reason why this attacking strategy becomes roughly the same as the random attacking one after a few iterations. The relative behaviour of the evolution of the giant component with respect to structure-based element removals (b_k, c_k and d_k) is consistent with the results presented in [52].

Figure **4-2**(b) plots the size of the second largest component of the graph C_2, which reveals, as expected, that the d_k and b_k attacking policies generate in a couple of iterations a new cluster composed by a significant portion of nodes (peaking roughly at 40 % of the nodes), while random, S_B and c_k focal methods generate smaller subgraphs.

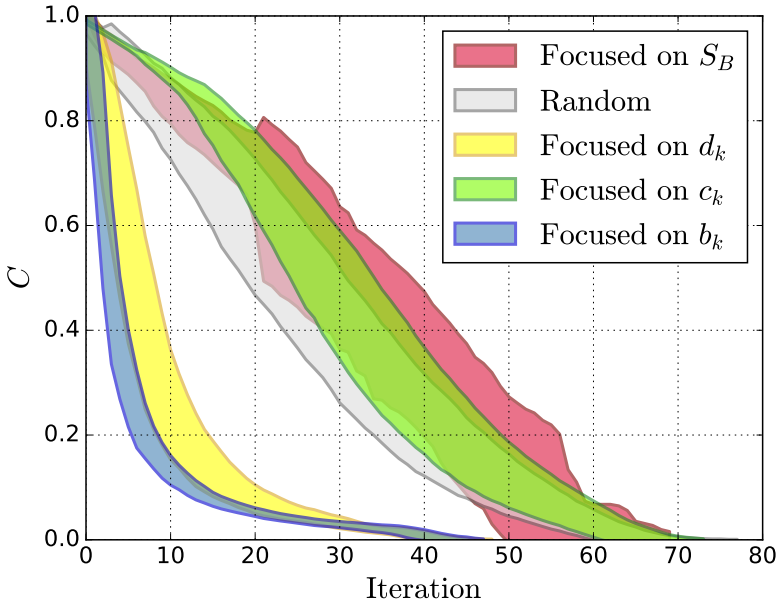

(a) Giant component of the network.

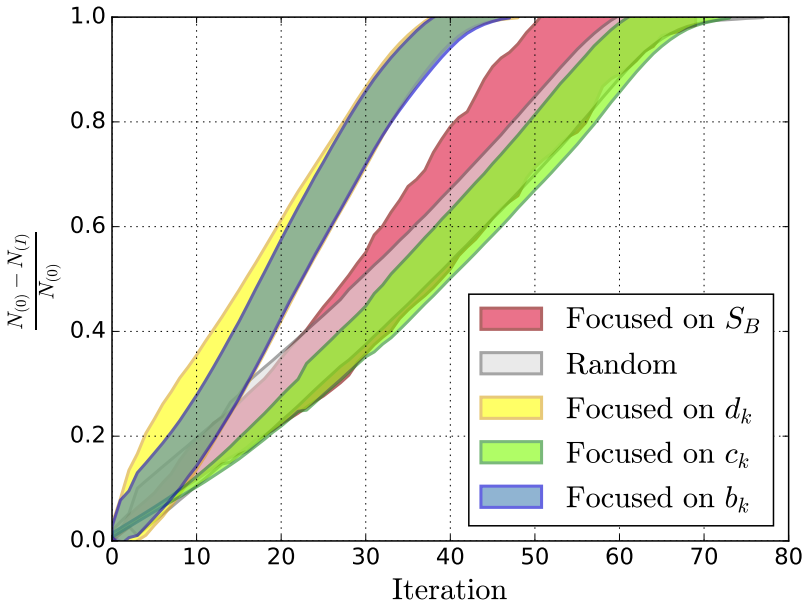

(b) Removed component of the network.

Figure 4-1.: Evolution in the structure of the randomly grown synthetic power grids subject to the nodal elimination algorithm. The shading accounts for the standard deviation calculated over 10 realizations for the S_B-focused methodology and 500 realizations for the other attacking schemes.

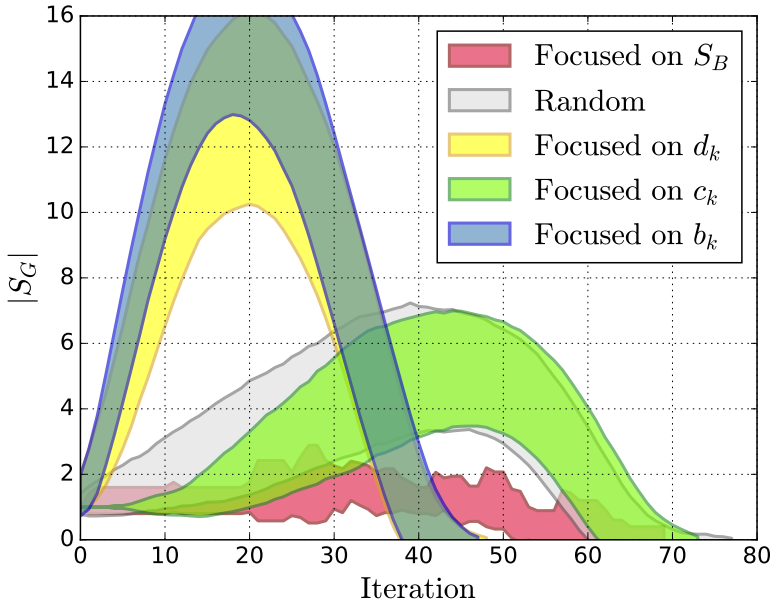

(a) Amount of operational clusters in the network.

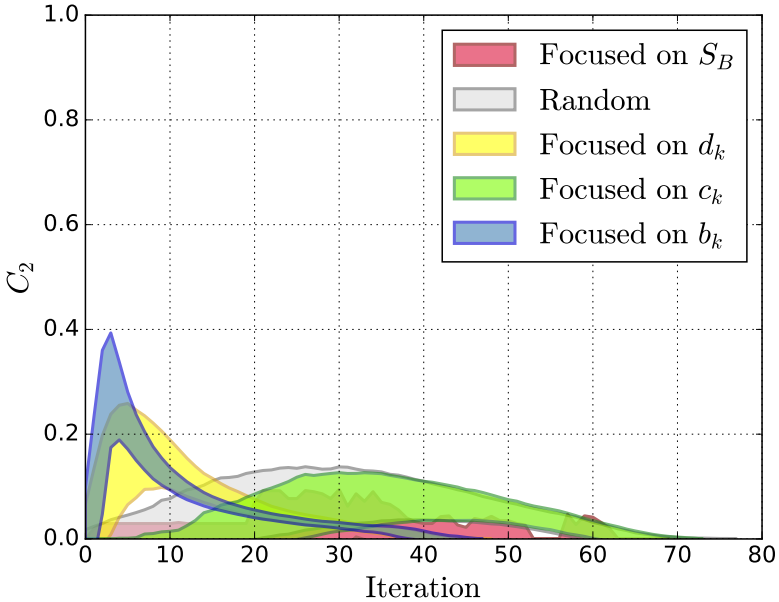

(b) Second largest component of the network.

Figure 4-2.: Evolution in the structure of the randomly grown synthetic power grids subject to the nodal elimination algorithm. The shading accounts for the standard deviation calculated over 10 realizations for the S_B-focused methodology and 500 realizations for the other attacking schemes.

Regarding the S_B-focused attacking, a very similar behaviour to that of the random attacks is observed, except in Figure **4-2**(a), where S_B attacks produce the smallest amount of clusters. This is likely related to the observed phenomenon in [31], where nodes located on dead-tree arrangements were found to exhibit, in general, a lower SNBS than the rest of the nodes, being the inner tree nodes the most critical ones. As these are some of the nodes that are more likely to be removed first under S_B focal attacks, the graph does not segregate on multiple clusters that easily.

Let us consider *weak nodes* as those that exhibit a SNBS lower than 0.4, then the fraction of weak nodes can be expressed as:

$$\eta_w(I) = \frac{N_w(I)}{N(I)} \tag{4-2}$$

where $N_w(I)$ and $N(I)$ are respectively the number of weak nodes and the total amount of nodes in the graph at iteration I of the resilience testing algorithm. Figure **4-3** shows the behaviour of the fraction of weak nodes η_w after each iteration for the S_B-focused attacking algorithm. From this figure, something that is not intuitive can be observed: in general, removing the most vulnerable nodes in the network is causing an overall reduction of the stability of the whole network. This implies that, although attacking nodes with a poor SNBS will not lead to blackout of the network faster than other strategies, it is making the whole grid more prone to dynamical disturbances in oscillation frequency and phase angle. It is worth noting that, results on Figure **4-3** are statistically less reliable in the last iterations due to the fact that each power grid reaches total blackout at a different iteration value in general, thus, last iterations are not averaging necessarily over 10 realizations as the first iterations are.

Figure **4-4** shows the amount of generators N_g and consumers N_c after each iteration, and it allows to see how the node elimination is working: in average, both, consumers and generators are being eliminated at the same rate, this leads to believe that every new cluster created in the network preserves a comparable number of both kind of nodes and that homogeneity makes the total destruction of said cluster less likely. This also explains why, in average, the transition to blackout for the S_B-method is very similar to that of the random case on Figure **4-1**(a).

Finally, for the data obtained from the S_B-focused simultions, the Pearson correlation is computed for the relationship between the $S_B^{(k)}$ and the structural parameters of each node: b_k, c_k, d_k and the power P_k. The results of this statistical test are presented in table **4-1**, where σ is the Pearson correlation coefficient and p_{val} is the corresponding two-tailed p-value.

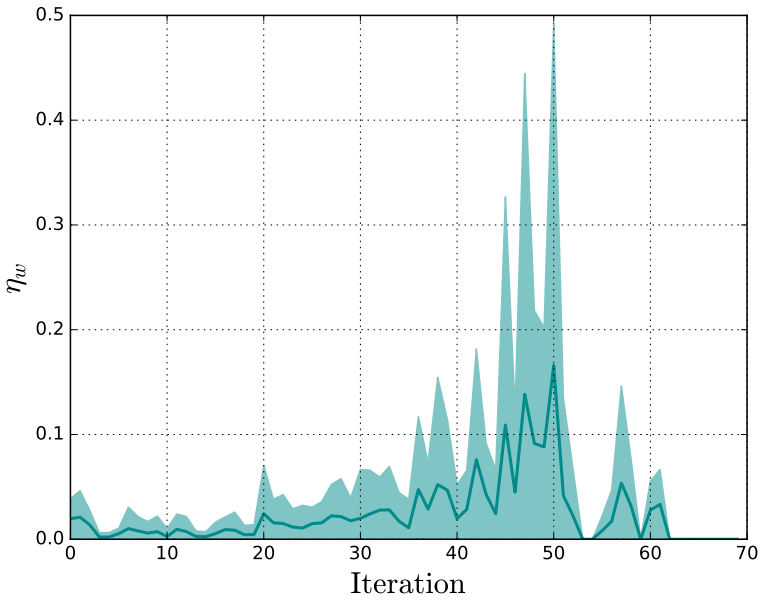

Figure 4-3.: Fraction of weak nodes on each iteration of the node removal algorithm on synthetic power grids. The shading accounts for the standard deviation over 10 random realizations. Note that the statistical significance of the trace is lower at the last iterations, due to each realization reaching total blackout at different times.

Table 4-1.: Correlation between $S_B^{(k)}$ and structural parameters of the synthetic power grids.

	b_k	c_k	d_k	P_k
σ	0.037	0.004	-0.056	-0.221
p_{val}	2.9×10^{-10}	4.6×10^{-1}	7.7×10^{-22}	0.0

After this testing, a small but significant negative correlation is found between the basin stability of a node and the power it produces or drains from the network with $\sigma = -0.22$ and $p_{val} = 0.0$. This suggests that a higher value of the power in a node reduces its stability to non-local frequency disturbances. For the other structural parameters, negligible correlation is found, so no conclusion can be extracted from this.

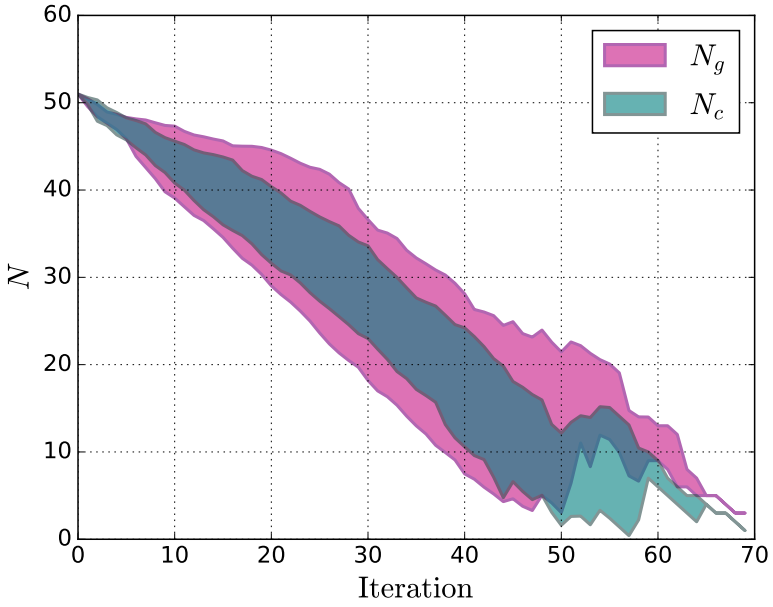

Figure 4-4.: Number of consumers N_c and generators N_g existing in the graph on each iteration of the S_B-focused removal algorithm. The shading accounts for the standard deviation over the 10 random realizations.

4.3.2. Line Resilience

Figure **4-5** presents the evolution of the graph under the edge removal procedure. The difference between the random and focal schemes is remarkable on these simulations: by focusing attacks on transmission lines with higher loads $\Delta_\theta(i,j)$, the size of the power grid goes down rapidly and reaches total blackout faster than other attacking schemes.

By focusing on lines with a higher e_k, the sparsity of the graph grows rapidly and many small isolated but functional clusters form, as appreciated in Figure **4-6**(a), where the average number of clusters for e_k can even be twice the amount seen in the random case and almost three times the $\Delta_\theta(i,j)$ case.

It is also worth noting that the maximum size of C_2 shown in Figure **4-6**(b) is identical to that observed in the node removal experiment in Figure **4-2**(b), which is $\approx 40\,\%$, that should be related to the parameters used in the power grid construction algorithm, and mainly, with the redundant link probabilities p and q and the redundancy exponent r, since they tune the local and global redundancy of the generated graph.

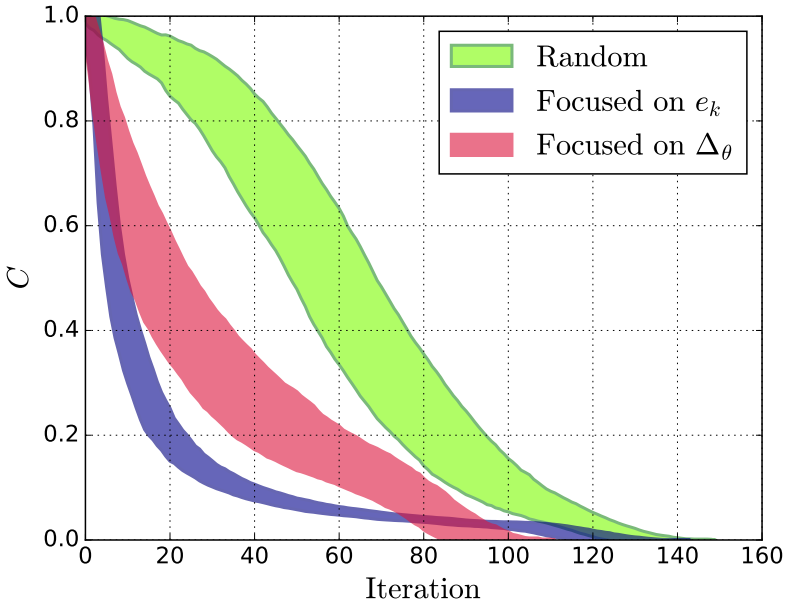

(a) Giant component of the network.

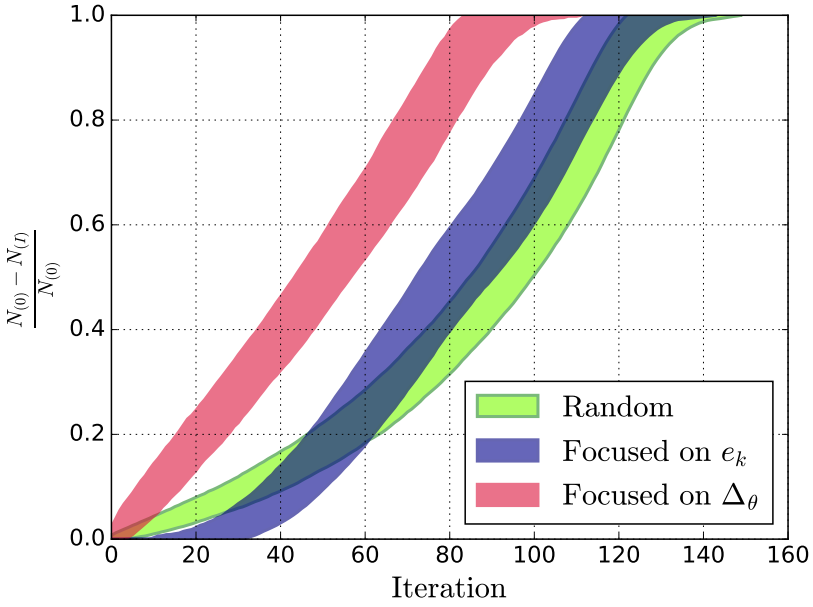

(b) Removed component of the network.

Figure 4-5.: Evolution in the structure of the randomly grown synthetic power grids subject to the edge elimination algorithm. The shading accounts for the standard deviation calculated over 500 realizations.

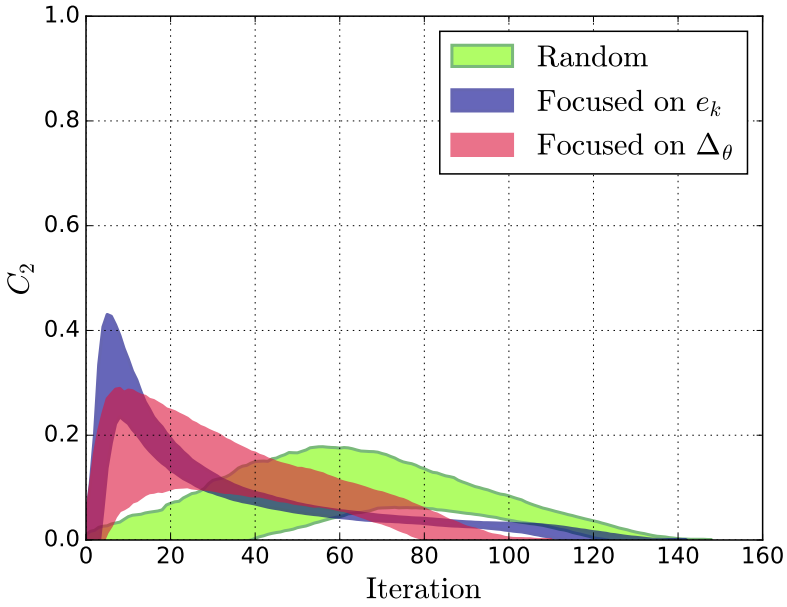

(a) Second largest component of the network.

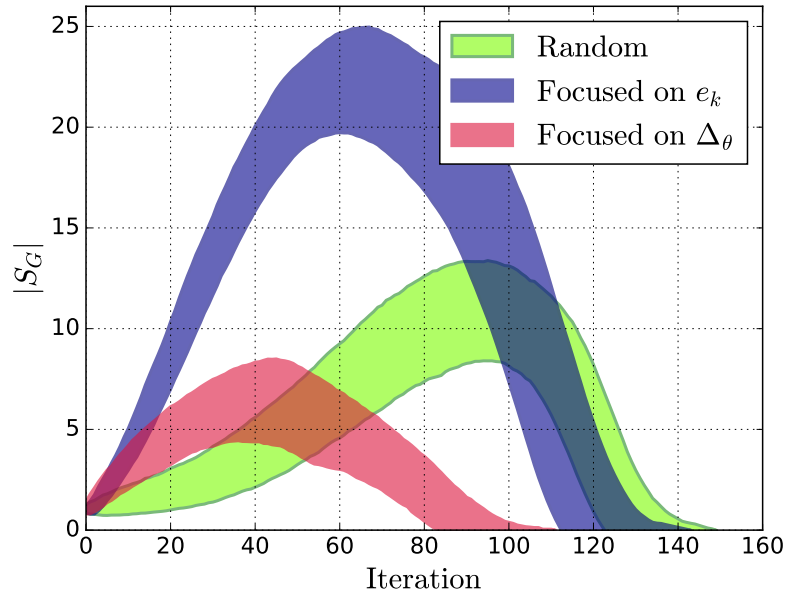

(b) Amount of operational clusters in the network.

Figure 4-6.: Evolution in the structure of the randomly grown synthetic power grids subject to the edge elimination algorithm. The shading accounts for the standard deviation calculated over 500 realizations.

4.3.3. Phase Transitions

From the percolation-inspired procedure employed here, two "phase transitions" could be analysed:

- **Transition T_1:** This transition occurs in the iteration when the graph is divided into multiple functional subgraphs for the first time (turning from a connected graph to an unconnected graph). This transition can be observed in either Figure **4-2**(a) or **4-6**(a) when the second largest component switches from zero to a different value.

- **Transition T_2:** The final iteration of the algorithm, when the power grid goes to complete blackout. As explained earlier, it can be observed in Figure **4-1**(b) or **4-5**(b) when the removed component reaches 1.

For each elimination method, table **4-2** summarizes the value of T_1 and T_2 as computed from the mean traces in the mentioned figures. Recall that each value is averaged over 500 simulations, except S_B^k which is over 10 realizations.

Table 4-2.: Average value of T_1 and T_2 for the resilience testing algorithm in the synthetic power grids.

	Random Node	b_k	c_k	d_k	S_B^k	**Random Edge**	e_k	Δ_θ
T_1	10.20	2.35	19.58	2.50	27.00	17.48	4.61	4.14
T_2	61.62	39.91	63.22	39.02	54.30	125.71	116.83	87.33

An important analysis is how the critical iterations for which these transitions occur, are affected for the parameters in the system. In that regard, for the line resilience procedure, T_1 and T_2 were calculated over variations in the coupling strength k as shown in Figure **4-7**. For T_1 on panel (a), no clear tendency is observed, besides the expected fact that this transition is, in general, higher for the random method than for other elimination strategies. Panel (b) however shows something interesting for T_2: for any value of k, attacking the most vulnerable edges based on the dynamics (Δ_θ) produces the fastest transition to blackout in the synthetic power grids, while attacking randomly produces, in general, the slowest transition. Furthermore, this transition seems to slowly increase as k is increased, which means that a higher coupling coefficient not only increases synchronization stability but also structural resilience in this focused attacking framework.

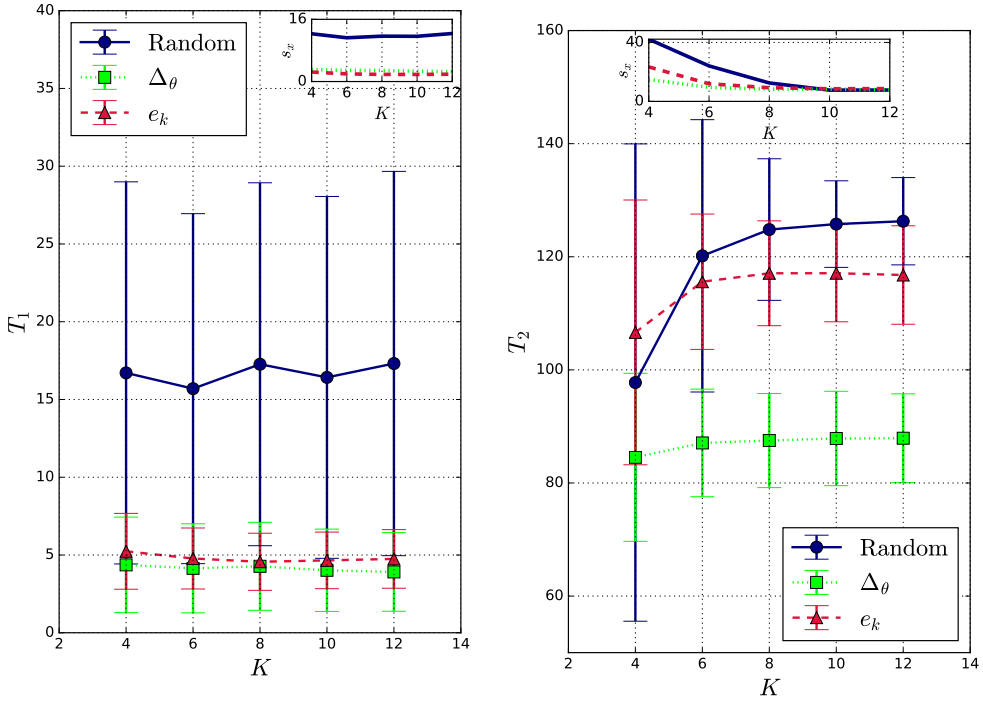

(a) T_1: Transition to unconnected graph.

(b) T_2: Transition to blackout.

Figure 4-7.: Phase transitions T_1 and T_2 for the line resilience testing algorithm over the synthetic power grids. Error bars account for the standard deviation over 20 random realizations.

The same analysis is performed for the node elimination algorithm, as shown in Figure **4-8**. It should be noted that by decreasing K below 10, T_1 for the SNBS case becomes lower than the random case on average, hinting that the effect where weaker nodes are located mainly in inner-tree nodes is more noticeable when K is somewhat large, while for lower K, the weak nodes are spread all around the graph. This is understandable since, in general, it can be expected that the basin stability of a node is increased when the coupling of the network is enhanced (this behavior however is not monotonic for all nodes, as pointed out in [73, 88]). For the random and the topology-dependant elimination methods, no tendency is observed for T_1 when varying K.

T_2 on the other hand shows an evident increase for any removal method when the coupling strength is increased. As shown in figure **4-8**(b), random and topological-based elimination methods seem to reach a plateau when K is sufficiently high. This reduction in the variability of T_2 is because, for a higher K, the network becomes more robust to lose clusters due to lack of synchronization (step 5 in the algorithm) and thus, clusters are removed merely by

the lack of generators and consumers (step 3) or by single elimination (step 1 and 2). The number of attacks required to reach blackout on either of those two cases depends mostly on the initial construction of the network, therefore it should not vary significantly among multiple experiments. The SNBS removal depends on the system dynamics, thus its curve does not flat as the others for the observed range, however it is expected to behave in the same way for a significantly higher K when the set point in any node becomes globally stable in Π.

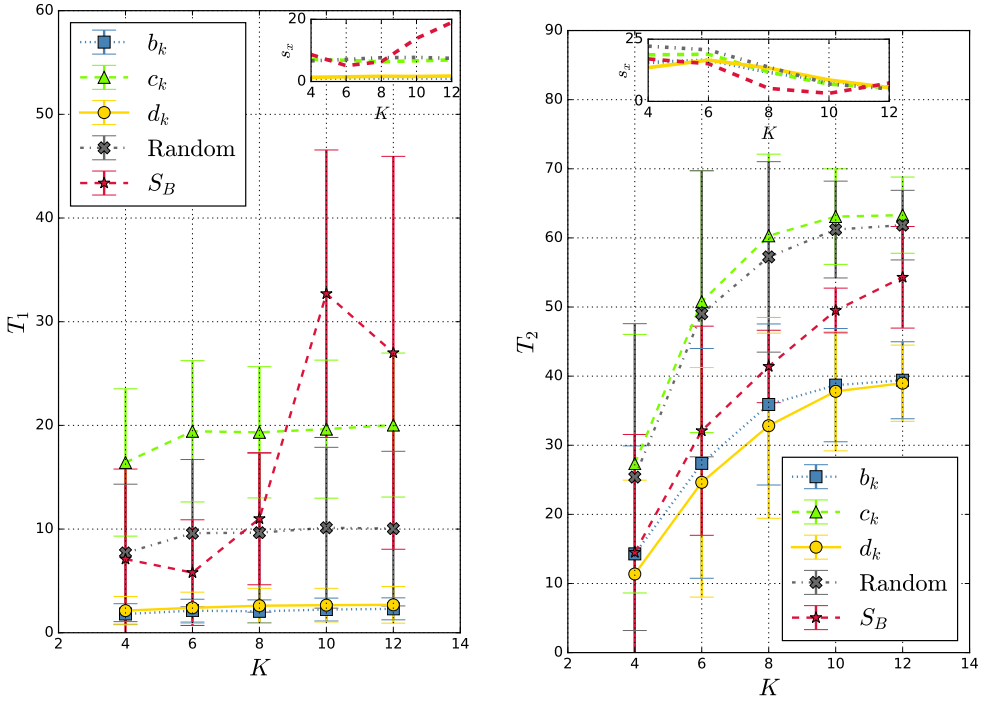

(a) T_1: Transition to unconnected graph.

(b) T_2: Transition to blackout.

Figure 4-8.: Phase transitions T_1 and T_2 for the node resilience testing algorithm over the synthetic power grids. Error bars account for the standard deviation over 10 random realizations.

Some interesting elements have been brought up concerning these results, and they will be wrapped up in the next chapter once the same procedure is performed over a real-world power grid case, namely, the Colombian power transmission network.

5. Colombian Power Grid

5.1. Abstract

In this chapter, the theory developed previously will be used to analyse the specific case of the Colombian power grid topology. Weak components of the network will be identified and the resilience of the system in general will be tested to cascade failures induced through the percolation-inspired simulations.

5.2. General Stability of the Network

In the following, the topology of $G(\vartheta, \varepsilon)$ is taken from the Colombian National Transmission System [95], a power grid composed of 158 edges and 102 nodes (28 of them are generators and 74 are consumers). From those 28 generators, 17 are hydroelectric while 11 are thermoelectric. In Figure **5-1**, (a) it is shown the topology of the network with the tree-like node classification introduced in section 2.5. Panels (b)-(e) present distributions for the classic centrality measures of the graph used throughout this document: node degree, clustering coefficient, node betweenness and edge betweenness centrality. Panels (f) and (g) display the behaviour of $\theta(t)$ and $\dot{\theta}(t)$ for every oscillator when the system converges from a random state to a frequency synchronized state.

In the following analysis, the power distribution for generator machines (P_k, $\forall k \in \vartheta_g$) and the power line capacity of each transmission line (K_{ij}, $\forall (i,j) \in \varepsilon$), were extracted from [95] and expressed in [p.u.] with a base power of 100 MW. In addition, for generators, which can be either hydroelectric or thermoelectric, a capacity factor of 60 % and 10 % was assumed, respectively, in order to emulate normal operation conditions of the power grid. For consumer nodes, an equal power demand was assumed, such that power balance (2-47) remains true. Finally, damping for every node is set to $\alpha_i = 0.1$. Under this set-up, Figure **5-2** describes the power distribution for power generators and transmission lines capacity in the Colombian power grid.

For this particular example, let us write the second-order Kuramoto model with a slight

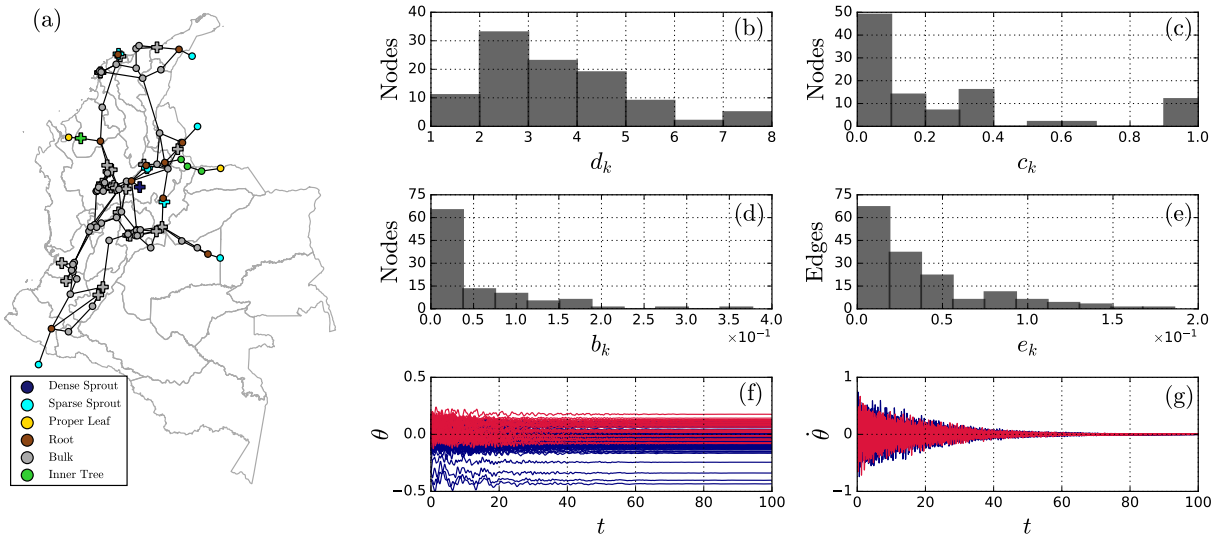

Figure 5-1.: Colombian Power Grid: (a) Topology of the network with $N = 102$ and $M = 158$. Generating nodes $N_g = 28$ (plus symbols) and $N_c = 74$ consumer nodes (circle symbols). (b)-(e) Distribution of the node degree d_k, clustering coefficient c_k, node betweenness centrality b_k and edge betweenness centrality e_k. (f)-(g) Time trace of the phases and phase velocities of each oscillator when the grid converges to a frequency synchronized state (red lines: generators, blue lines: consumers).

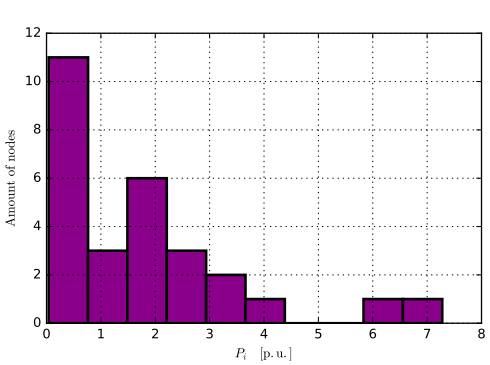

(a) Power distribution in generators.

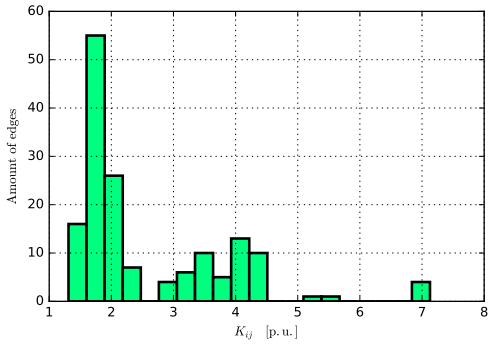

(b) Power capacity distribution for transmission lines.

Figure 5-2.: Distribution of parameters P_i for power generators and K_{ij} for the edges in the Colombian power grid.

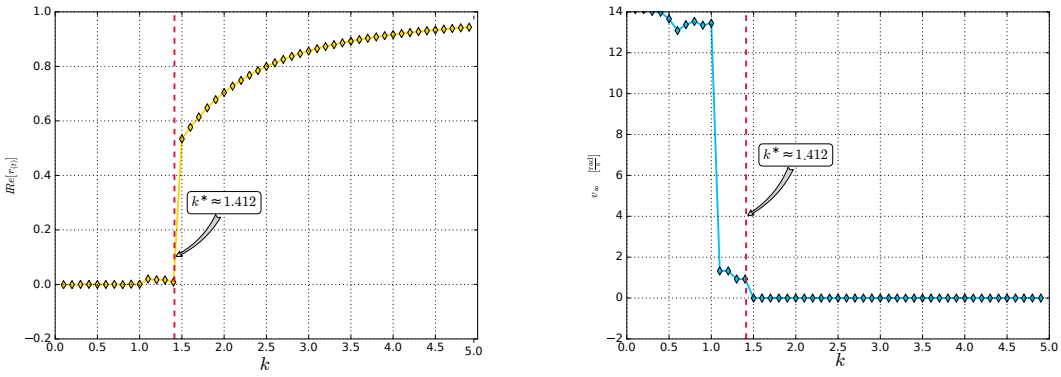

(a) Real part of the order parameter. (b) Average speed.

Figure 5-3.: Synchronization profile for the Colombian power grid with real power parameters. Red dashed vertical line marks the critical coupling as estimated through Equation (3-16).

adjustment in notation as:

$$\ddot{\theta}_{j(t)} = P_j - \alpha_j \dot{\theta}_{j(t)} + k \sum_{i}^{N} K_{ji} \sin(\theta_{i(t)} - \theta_{j(t)}) \tag{5-1}$$

Where just a constant k was introduced to allow the investigation of the critical coupling of the Colombian power grid. Figure **5-3** does precisely that by plotting the real part of the order parameter and the average speed of the ensemble as a function of k. It is found that given the parameters chosen, the critical coupling is found around $k_c \approx 1.412$ as estimated through Equation (3-16) and which perfectly matches the simulated trace. For this discussion, the coupling strength will be set to $k = 1.5$ to guarantee that the system operates inside the synchronized regime.

Finally, let us define the load for a transmission line that connects node j to i as:

$$F_{ij} = \sum_{i}^{N} K_{ji} \sin(\theta_{i(t)} - \theta_{j(t)}) \tag{5-2}$$

The power grid is then analysed by inspecting the load in the transmission lines, as well as the basin stability and the recovery time for the nodes in Figure **5-4**. On this specific example, SNBS and recovery time was estimated with $I_C = 500$ and $I_C = 100$, respectively. Those nodes for which 100 stable trajectories to compute t_r could not be found are black coloured in Figure **5-4**(c), and thus excluded from the recovery time analysis.

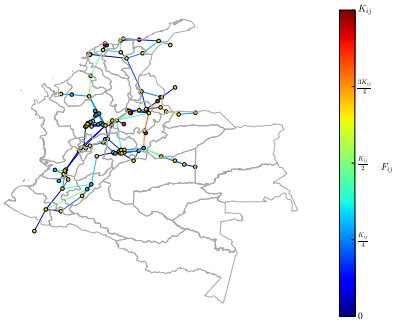

(a) Line load distribution. Blue node: hydroelectric generator; red node: thermoelectric generator; yellow node: consumer.

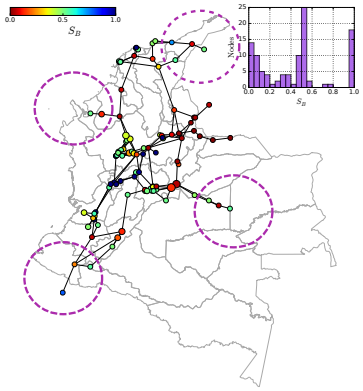

(b) Basin stability distribution.

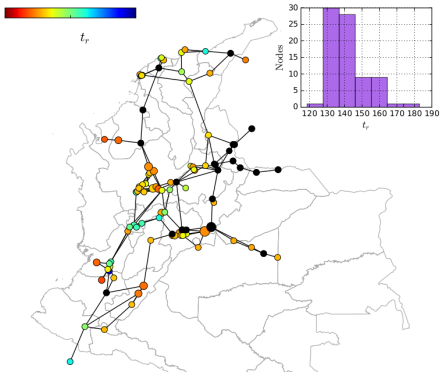

(c) Recovery time distribution.

Figure 5-4.: Dynamical characteristics of the nodes and edges in the Colombian power grid, modeled with realistic parameters for P and K.

Some key features about the Colombian power grid can be observed in this Figure:

- From Figure **5-4**(a), it can be seen that most of the transmission lines have a low load level, but there are some exceptions, some critical links that should be taken into consideration since their high load levels imply that a random perturbation in the locally demanded or supplied power could lead to the line outage and potentially to cascading failures that would affect the network non-locally. As observed, those heavily loaded lines are mainly located in the eastern side of the network, in the regions of Boyacá, Santander and Norte de Santander. A shorter line in Antioquia has to be mentioned too.

- Synchronous machines located on the north-eastern side of the power grid are extremely susceptible to random disturbances, as appreciated in Figure **5-4**(b); this includes Boyacá, Santander, Norte de Santander and Arauca. Two significantly weak clusters are also distinguishable, one by the southwest, including Cauca, Nariño and Huila; the other is by the north, spanning through Córdoba, Sucre, Atlántico and Magdalena. There are also some interesting elements in the network which are marked by a dotted magenta circle. Those 4 regions include dead-tree topologies, which were discussed in [31], and the authors found that inner tree nodes usually had a lower SNBS than the proper leafs at the extreme of the tree, as clearly occurs here in the Colombian power grid too.

- In Figure **5-4**(c) it is reported that most of the nodes suppress large dynamical disturbances in $130 \sim 140$ time units, but a cluster of slow nodes is formed in the center of the grid, including the regions of Caldas, Quindío, Tolima and Antioquia. A definite relationship between t_r and the topology of the complex network is currently an open research problem in the state of the art.

5.3. Resilience Assessment

Now that the basic properties of the network have been described, the discussion is turned to how resilient to cascading failures the Colombian power grid actually is.

For the following numerical experiment, we only care about the topology of the network itself, thus homogeneous coupling will be assumed for every link in the network (in other words, K_{ij} takes values 1 or 0), power supplied by generators is set to $P_k = 1.0$, $\forall k \in \vartheta_g$, and the power drained by consumers is chosen such that there is a power balance in the network (Equation (2-47)). Under these assumptions, the new critical coupling of the network is estimated to $k_c \approx 1.51$, as illustrated in Figure **5-5**. In the following, $k = 12.0$ to allow for

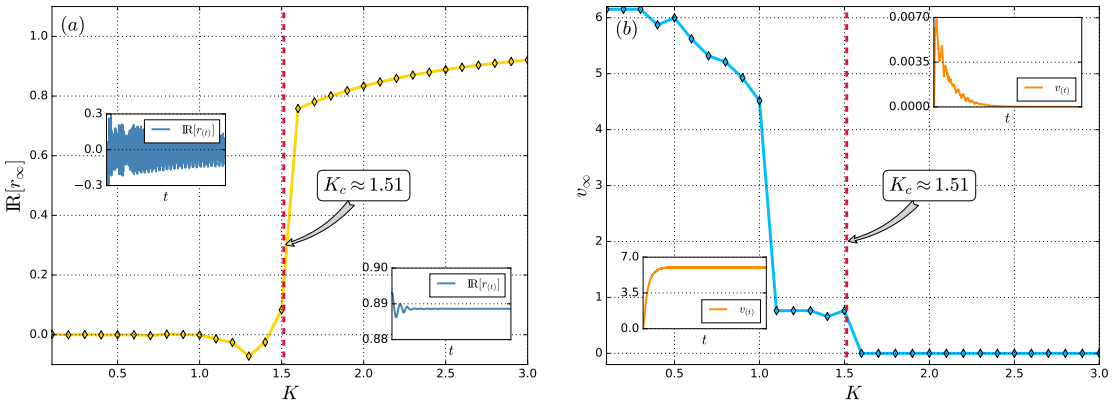

(a) Real part of the order parameter. (b) Average speed.

Figure 5-5.: Synchronization profile for the Colombian power grid with simplified parameters. Red dashed vertical line marks the critical coupling as estimated through Equation (3-16).

a synchronized state to exist.

5.3.1. Nodal Resilience

Figure **5-6** illustrates the algorithm for nodal resilience measurement under S_B-focused attacks. The transition from the frame (a) to (b) shows the formation of 2 independent clusters after removing one node. Note that in the frame (c) there is only one generator in the northern cluster, and interestingly, it has a very poor basin stability level, so when that node is removed from (c) to (d), the whole northern cluster goes to blackout. A different realization is presented in panels (e)-(h); note that from (g) to (h) it suffices to remove one node to bring the bigger cluster to blackout even though there would remain connected subgraphs with both generators and consumers. This occurs because the remaining cluster would have a topology that does not satisfy the synchronization condition (3-14) and thus it vanishes.

Results for the node percolation algorithm are presented in Figures **5-7** and **5-8**. It is surprising that besides the narrower standard deviation in every trace (which was to be expected considering that a lot of the randomness is reduced here when using a fixed complex network structure), every other behaviour related to the elimination based on b_k, c_k, d_k and even the random attacking method is identical to that observed in the randomly grown synthetic power grids from Figures **4-1** and **4-2**.

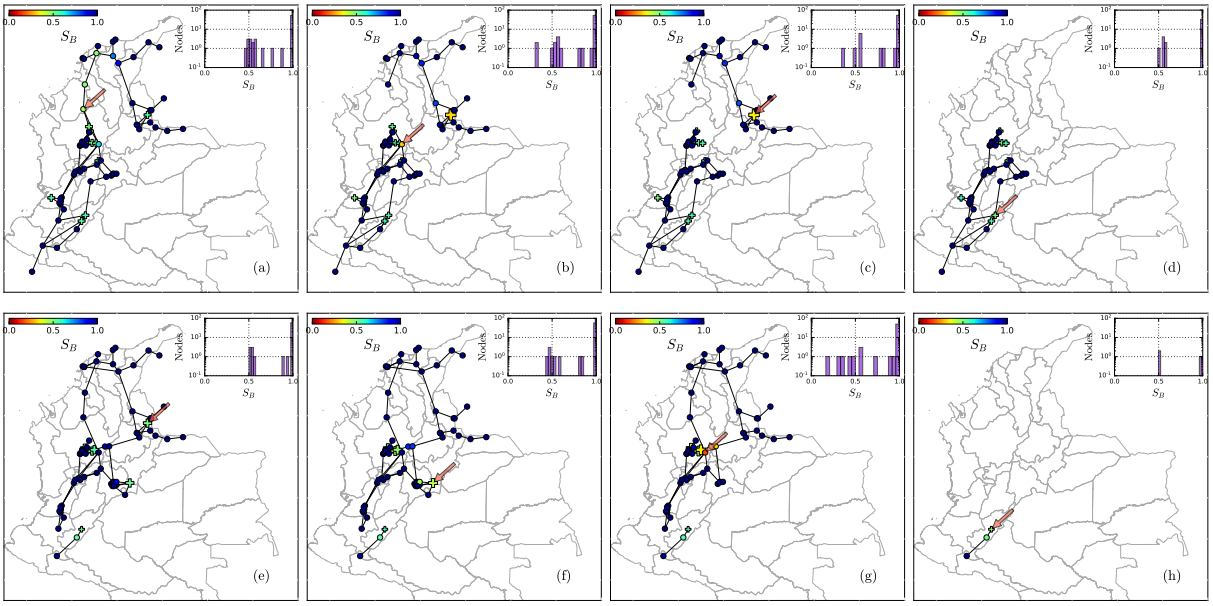

Figure 5-6.: Node removal algorithm under the focal attacking scheme. Circle nodes indicate consumers while crosses mean generators. Node color is mapped with the $S_B^{(i)}$ and the size of the node is proportional to the power P_i. The red arrow indicates the node that is going to be suppressed. Also, the inset shows the histogram of the basin stability for the whole network. One realization is presented in panels (a)-(d) and a different one in panels (e)-(h) in order to visualize two different mechanisms of cluster vanishing.

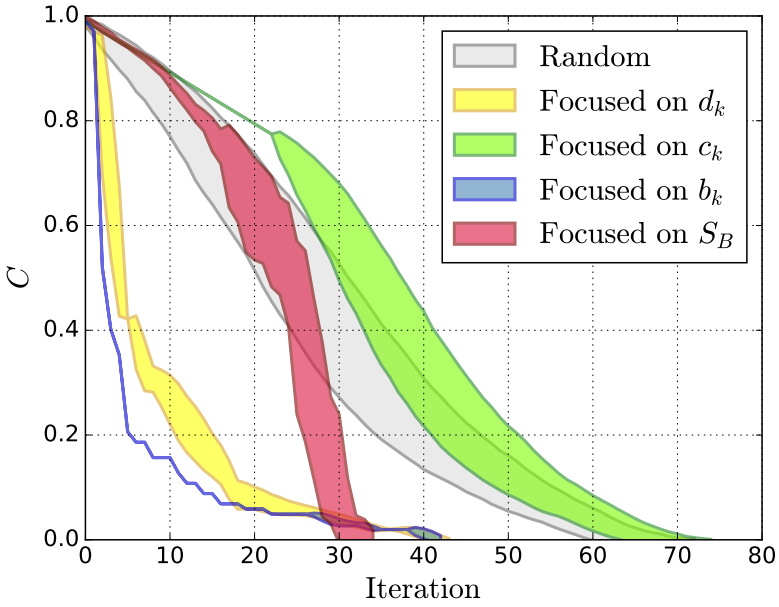

(a) Giant component of the network.

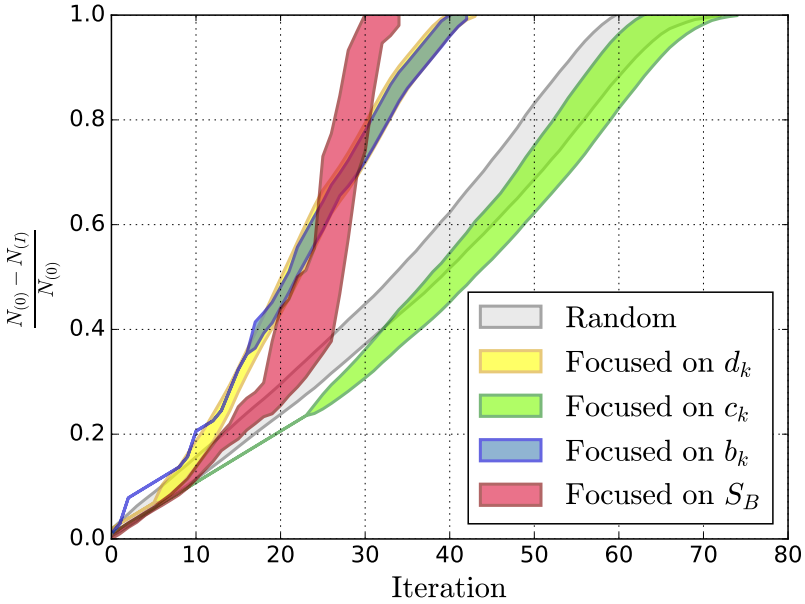

(b) Removed component of the network.

Figure 5-7.: Evolution in the structure of the Colombian power grid subject to the nodal elimination algorithm. The shading accounts for the standard deviation calculated over 5 realizations for the S_B-focused methodology and 500 realizations for the other attacking schemes.

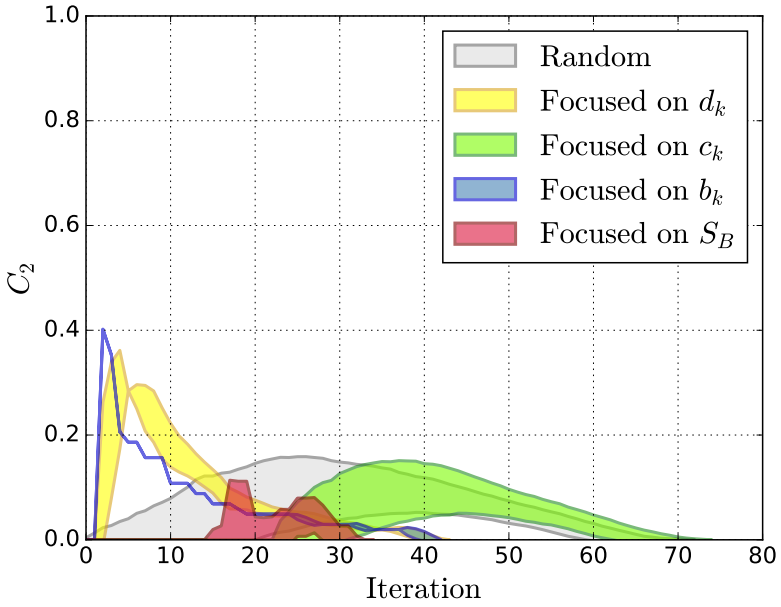

(a) Second largest component of the network.

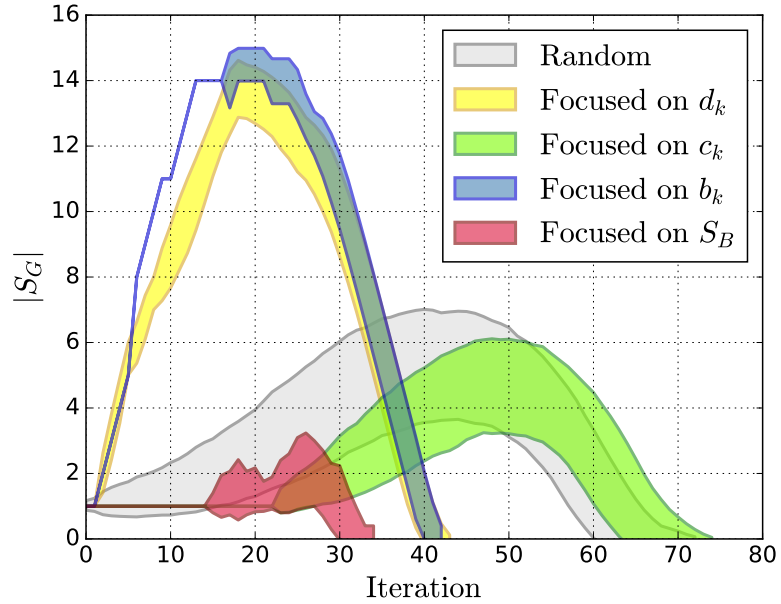

(b) Amount of operational clusters in the network.

Figure 5-8.: Evolution in the structure of the Colombian power grid subject to the nodal elimination algorithm. The shading accounts for the standard deviation calculated over 5 realizations for the S_B-focused methodology and 500 realizations for the other attacking schemes.

This confirms the fact that the algorithm proposed in [35] is indeed capable of reproducing real-world examples of networked power systems, but also reveals that an heterogeneous power distribution did not have, on average, a significant impact in the transition to blackout profile for these specific attacking schemes.

However, a major difference is observed when attacks are applied to the most vulnerable nodes based on S_B, which for the Colombian power grid produces a faster transition to the total blackout state of the network than just removing nodes at random, implying that there is indeed a relationship between the resilience of a node against dynamical disturbances (related to the SNBS) and the structural connectivity of the graph, at least for this specific network; a relationship that can not be easily extended to any other system.

Interestingly, as it is evident from Figure **5-8**(a), the transition to an unconnected graph composed of multiple functioning clusters (T_1) for the S_B percolation case, takes several iterations (about 15 iterations) and it occurs significantly closer to the total blackout transition (T_2 - about 30 iterations) than any other methodology. This behaviour is further complemented with Figure **5-8**(b), where the amount of independent clusters (subgraphs) in the network is also observed. For the case of c_k, the amount of clusters remain constant at 1 for roughly 21 iterations, and this is then followed by a behaviour very similar to that of the random elimination, once the clustering coefficient is roughly uniform for the whole network.

Figure **5-9** reveals that the behaviour observed for the synthetic networks, where the proportion of vulnerable nodes η_w in the grid increases after some node eliminations based on S_B also occurs for the Colombian case, which supports the idea of using this strategy for focal attacks as a way to reduce the general stability of the power grid.

On the other hand, from Figure **5-10** the rate at which consumers and generators are being eliminated from the grid and when compared with Figure **4-4** for synthetic power grids, a very different behaviour is observed. While for the random synthetic power grids it was observed that N_g and N_c go down at the same rate, for the Colombian power grid the decreasing slope for N_g is faster than that of N_c for the first iterations. Since the initial amount of generators is lower than the initial amount of consumers after some of the nodes in the former group have been removed from the graph, the resulting clusters are more likely to be consumers isolated without a connected generator, subsequently, these clusters go to blackout. This implies that the main reason why clusters are being suppressed from the Colombian grid is the absence of generators in them, and explains why the transition to total blackout in the S_B-focused method is the fastest in Figure **5-7**(b).

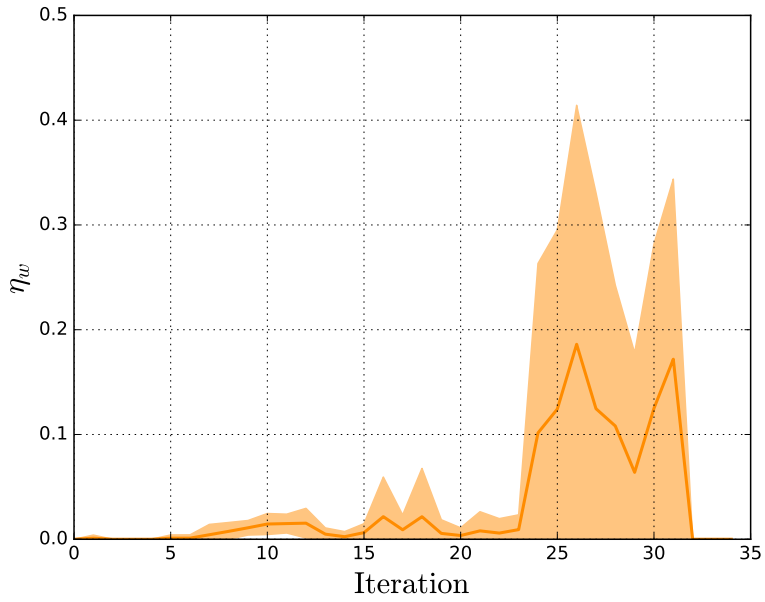

Figure 5-9.: Fraction of weak nodes on each iteration of the node removal algorithm on the Colombian power grid. The shading accounts for the standard deviation over 10 random realizations. Note that the statistical significance of the trace is lower at the last iterations, due to each realization reaching total blackout at different times.

Following the procedure described in section 4.3.1, it was calculated the Pearson correlation between the SNBS and the structure of the network and the results are described in Table **5-1**. Again, a significant negative correlation is found against the power parameter with $\sigma = -0.605$ and a $p_{val} = 0$. More analysis in this regard will be provided in section 5.4.

Table 5-1.: Correlation between $S_B^{(k)}$ and structural parameters of the Colombian power grid.

	$\boldsymbol{b_k}$	$\boldsymbol{c_k}$	$\boldsymbol{d_k}$	$\boldsymbol{P_k}$
$\boldsymbol{\sigma}$	0.027	-0.038	-0.005	-0.605
$\boldsymbol{p_{val}}$	3.5×10^{-5}	1.4×10^{-8}	4.3×10^{-1}	0.0

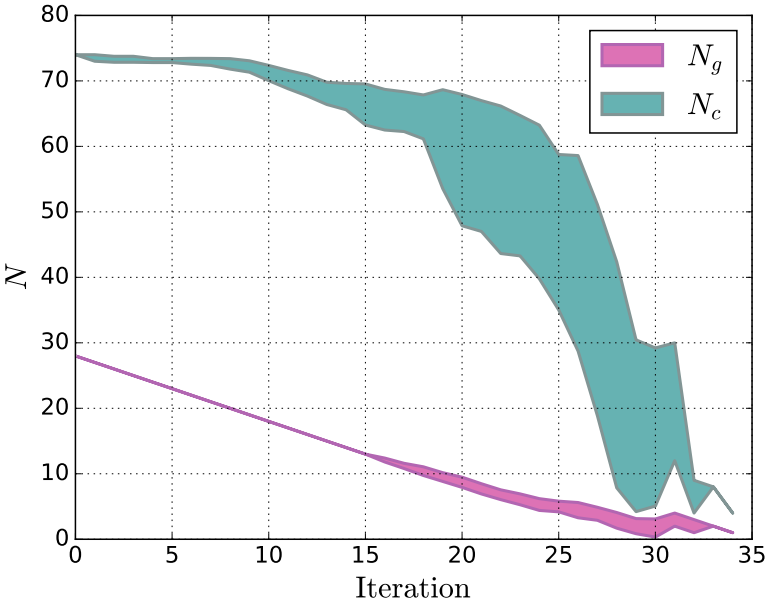

Figure 5-10.: Number of consumers N_c and generators N_g existing in the graph on each iteration of the S_B-focused removal algorithm. The shading accounts for the standard deviation over the 10 random realizations.

5.3.2. Line Resilience

Similarly, Figure **5-11** shows the edge removal algorithm in action under Δ_θ-focused attacks. In the transition from panel (b) to (c), it can be appreciated that, after suppressing a very vulnerable transmission line, a significant cluster of isolated consumers in the east side of the network vanishes.

Figures **5-12** and **5-13** show the evolution of the structure of the Colombian graph subject to transmission line attacks. It is very surprising that the traces in these figures fit perfectly inside the standard deviations to those traces found for the synthetic power grids (Figures **4-5** and **4-6**). This implies that the Colombian power grid acts as a particular example of the synthetic power grids generation algorithm and more importantly, the fact that the Colombian case has a way lower number of generators than consumers, did not have an impact in the location of transitions T_1 and T_2 for the edge removal algorithm. On average then, the dynamical parameter Δ_θ seems to be unrelated to the power distribution in the nodes.

Table **5-2** summarizes the average value of the transitions for the removal algorithm applied to the Colombian power grid.

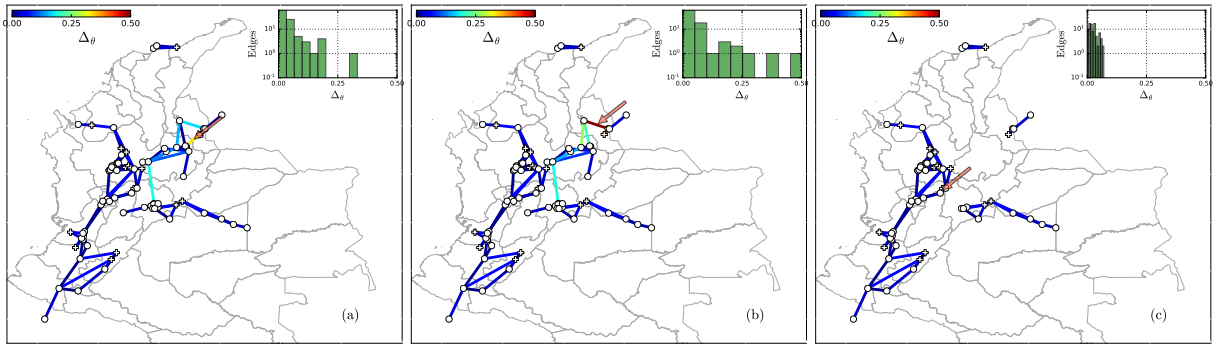

Figure 5-11.: Edge removal algorithm under the focal attacking scheme. Edge color is mapped with the Δ_θ of the nodes it connects. The red arrow indicates the edge that is going to be suppressed. Also, the inset shows the histogram of the phase differences for the whole network.

Table 5-2.: Average value of T_1 and T_2 for the resilience testing algorithm in the Colombian power grid.

	Random Node	b_k	c_k	d_k	S_B^k	**Random Edge**	e_k	Δ_θ
T_1	14.41	3.00	28.77	3.18	20.60	29.12	3.00	7.00
T_2	61.92	40.85	65.03	40.54	29.80	131.14	117.91	77.00

5.4. Basin Stability in Generators

As mentioned in the percolation algorithm, the power supplied by each generator is modified during the execution in order to maintain the power balance in the grid. Figure **5-14** shows the SNBS of each generator node in the complex network as a function of its power parameter. This figure is complemented by the results obtained in Tables **5-1** and **4-1** where a clear negative correlation was found between these two quantities for both experiments.

For both study cases: the Colombian power grid or the randomly grown synthetic power grids, it can be observed that, as the power of the node increases, its stability diminishes; this comes from the fact that P acts as a measure of the "stress" in the node, that is, the energy demand that it needs to satisfy. Having to provide energy for a higher amount of consumer nodes, a generator becomes then more susceptible to random perturbations, as indicated by the reduction on $S_B^{(i)}$. This can be contrasted with the results presented in [23], where it was found that, by distributing the demand among multiple small power generators, instead of a few big power plants, the value of the critical coupling K_c diminishes, thus synchronization is favoured, but for disturbances applied to power consumption, the most robust performance was found when there is a mixture of both, small and big power generators.

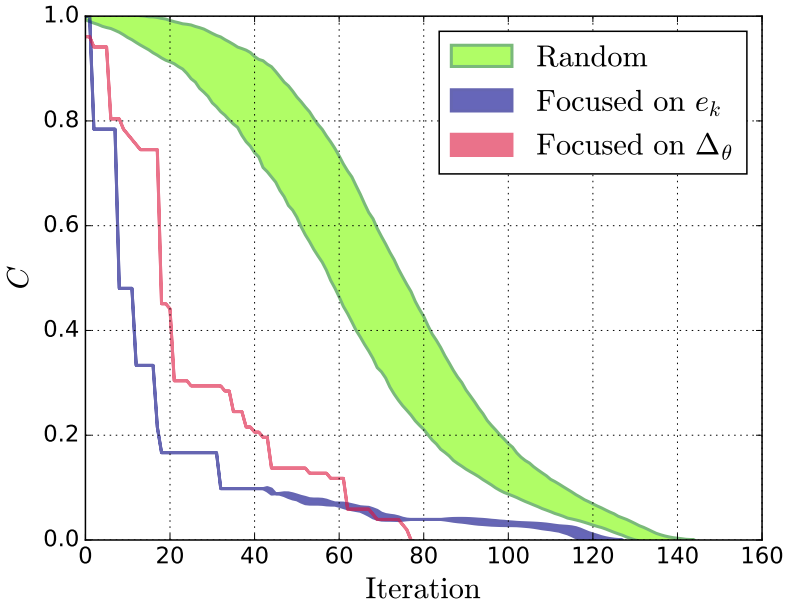

(a) Giant component of the network.

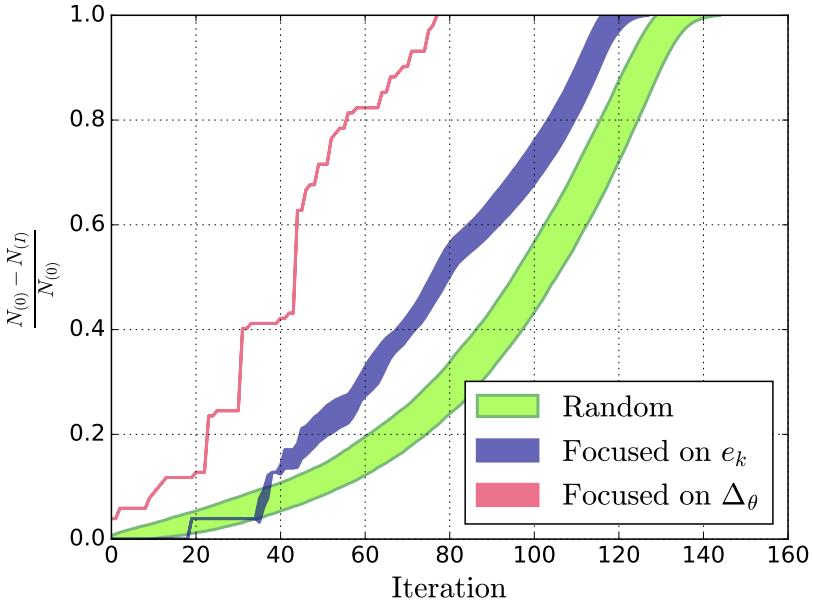

(b) Removed component of the network.

Figure 5-12.: Evolution in the structure of the Colombian power grid subject to the edge elimination algorithm. The shading accounts for the standard deviation calculated over 500 realizations.

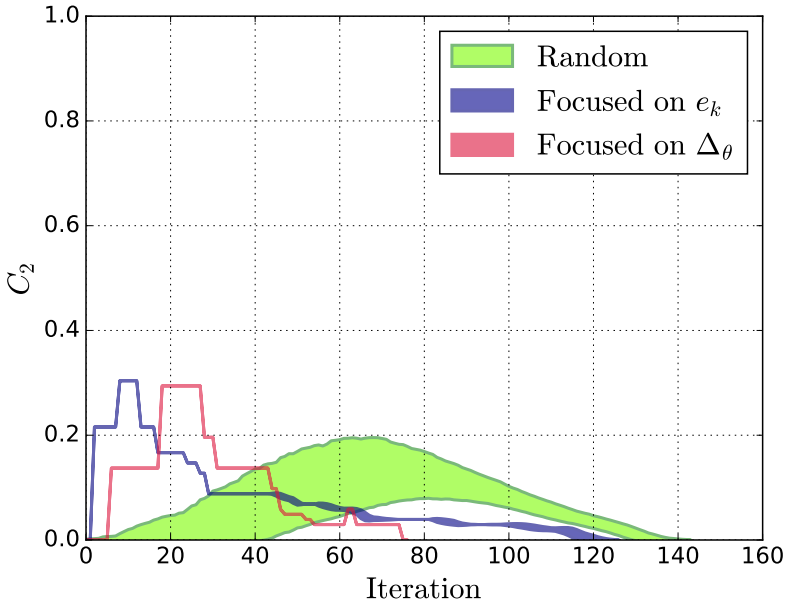

(a) Second largest component of the network.

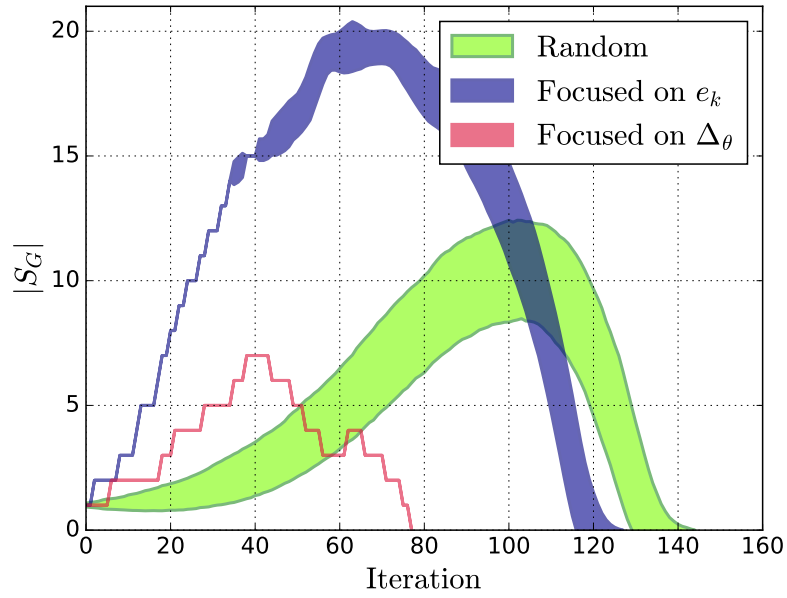

(b) Amount of operational clusters in the network.

Figure 5-13.: Evolution in the structure of the Colombian power grid subject to the edge elimination algorithm. The shading accounts for the standard deviation calculated over 500 realizations.

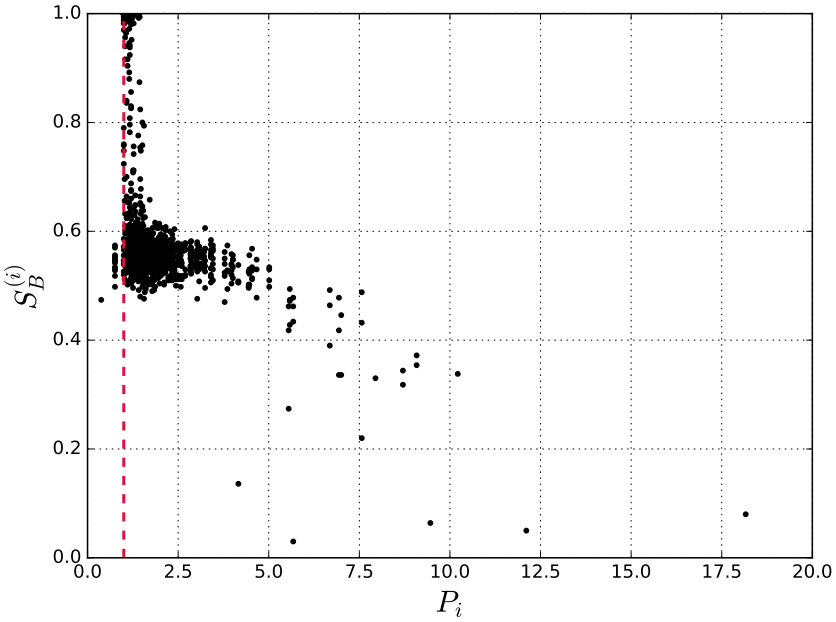

(a) Colombian power grid (Pearson correlation: $\sigma = -0.605$, $p_{val} = 0$).

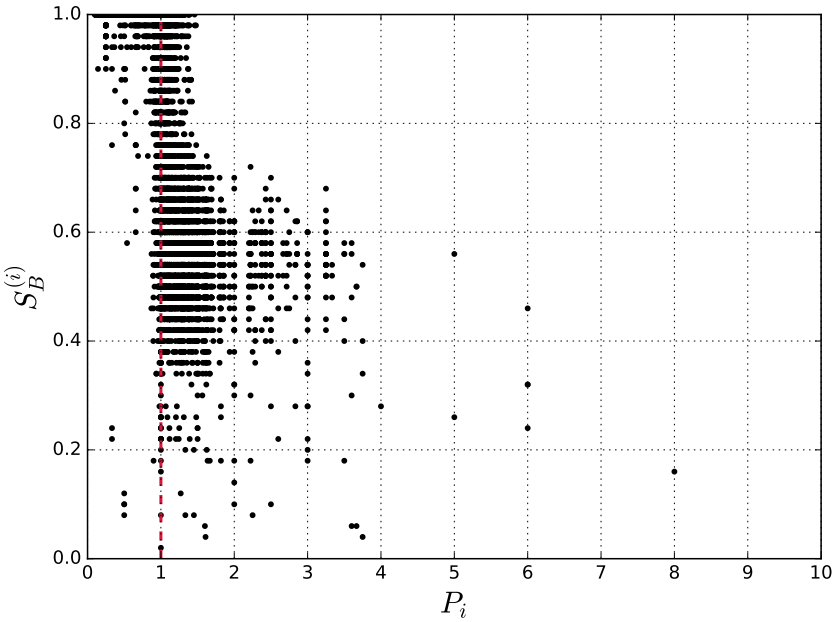

(b) Synthetic power grids (Pearson correlation: $\sigma = -0.22$, $p_{val} = 0.0$).

Figure 5-14.: SNBS of each generator node as a function of the power it supplies to the network. Red dashed line marks the initial set power $P = 1.0$.

6. Conclusions

In this document, an algorithm was proposed to test the resilience of power grids against structural failures. Our approach differs from others found in the literature since it takes into consideration dynamical stability against random non-local disturbances to describe nodal vulnerability, as well as linear stability of phase differences to compute edge vulnerability. The sequential elimination of elements in the network based on these dynamical vulnerabilities was also compared with the same procedure applied to structural vulnerabilities, which were defined in terms of connectivity patterns in the topology of the graph. This allowed extracting some interesting findings which will be discussed in the following.

First of all, focusing nodal attacks on redundantly connected nodes, such as those with the highest clustering coefficient, is obviously the least efficient strategy, pairing with the random removal; the blackout transition T_2 for both is always the highest, meaning that they require more attacks in order to destroy the whole network. Similarly, the giant component of the graph reduces at the slowest rate, since dividing the graph into multiple operational clusters is not likely until the redundant links are removed from the network. Eventually, both methods become essentially the same, once the clustering coefficient for the whole grid is uniform.

The most efficient way to reduce the size of the giant component of the network is, as expected, to attack the most central nodes, either those with the highest degree or betweenness; when these bulk nodes are removed, the graph rapidly segregates into multiple perfectly operational clusters. In other words, the transition to an unconnected graph T_1 is always the lowest for these methods.

For the case of node elimination based on basin stability, it was found that the transition to blackout T_2 in the randomly grown synthetic power grids did not differ significantly to that found for the random removal approach. However, in the specific case of the Colombian power grid, this method proved to be the most efficient to bring the whole network to total blackout. Other experiments based on the structure of the network exhibited the same behaviour for both, the synthetic grids and the Colombian case, suggesting that the only key difference between both test cases is the power distribution: for the synthetic grids the power was initially distributed uniformly, with an equal number of generators and consumers, but for the Colombian case only $27\,\%$ of the initial nodes are generators, and the rest consumers.

This power homogeneity in the synthetic grids then is enhancing the resilience of the graph, and this was confirmed when it was observed that for the Colombian grid, the first nodes to be removed are generators, leading to higher stress in the remaining power plants: a few generators will have to increase drastically the power they produce in order to balance the demand. In addition, this power increase in the generators will reduce their basin stability, that is, it will make them more prone to dynamical random disturbances in oscillatory frequency, as noted in the last chapter. This is an important finding, no correlation has yet been reported between the single node basin stability and the power supplied or drained by the node in the literature.

Interestingly, the number of weak nodes in the power grid (nodes with a low basin stability level), was found to increase during the node removal procedure focused on basin stability for both test cases. This implies that this attacking strategy is useful to undermine the general dynamical stability of the power grid and make it more prone to frequency disturbances, even though, it does not necessarily propagate structural failures to larger proportions of the network (it depends on the number of generators, as explained in the previous item).

Regarding the line resilience testing performed, it was found that for either the Colombian power grid or the synthetic power grids, attacking highly central edges, as those with a high edge betweenness centrality, the graph segregates rapidly into multiple clusters and the giant component reduces abruptly. The transition to blackout, however, is not faster than random elimination. It is, as expected, a very similar behaviour to that found in node elimination through node betweenness. The elimination based on the dynamical measure of phase difference (Δ_θ) was found to be the most efficient in order to bring the whole network to blackout, and remarkably, this behaviour can be observed for any value tested of the maximum transfer capacity in transmission lines.

A parallel study in this work included a basic analysis of the topology for the Colombian power grid with more realistic parameters. From this analysis, some key features were extracted and should be considered for future work:

Heavily loaded transmission lines were found in the eastern part of the power grid. Those lines should be reinforced to increase their maximum power capacity or the topology around them should be reconsidered in order to reduce the risk of breaking synchronization.

In addition, an extremely weak cluster of nodes was found in the eastern part of the grid, and two significantly weak by the south-west and the north, respectively. Those nodes are highly vulnerable to random frequency disturbances; it is recommended to include more regular connection topologies in this region and small cycles in order to raise the general basin stability.

Finally, a cluster of nodes at the center of the grid exhibit slow responses when rejecting random disturbances, this should be observed in more detail since a slow node allows disturbances to propagate to the rest of the network even in a non-local way.

This work provides some ideas and an analysis framework that could lead to the design of future power grids, aiming for robust and resilient systems. In order to achieve that, some work is still left open to research such as further exploring the hidden causes that are yielding the reduction of non-linear stability due to heterogeneous power distribution. Similarly, a more detailed study on the phase transitions T_1 and T_2, as well as the influence of structural parameters in these critical points, could potentially point in the right direction to design the most appropriate connectivity in a graph and parameter distribution such that resilience against cascading failures is optimized. More dynamical measures of vulnerability could also be incorporated in the removal algorithm; a particularly interesting one would be the multi-node basin stability [32] computed over the nearest-neighbours, as it would include information about the most vulnerable clusters, rather than individual elements. This would however impose a higher computational effort on a task that is already computationally expensive. Diffusivity of perturbations is also a promising feature to measure vulnerability to failure propagation [15].

To improve the analysis of the Colombian power grid, more information about the real world parameters could be introduced, like more precise capacity factors and demanded power by consumers. Extending the whole framework of synchronization to power grids where ohmic loss can't be neglected is also an open research problem in the current state of the art.

7. Academic Products

7.1. Journal Publication

The main findings discussed in this dissertation were presented in the following article:

- C. C. Galindo-González, D. Angulo-García, and G. Osorio, "Decreased resilience in power grids under dynamically induced vulnerabilities", *New Journal of Physics*, ISSN: 1367-2630, September 2020,
  URL `https://iopscience.iop.org/article/10.1088/1367-2630/abb962`,
  DOI `10.1088/1367-2630/abb962`

7.2. Conference Participation

Some initial results were also shared by the co-advisor, David Angulo, at the second Latin American Conference on Complex Networks (LANET), on august 2019, under the following talks:

- C. C. Galindo-González, D. Angulo-García, and G. Osorio, "Dynamical stability analysis of the Colombian Power Grid", *Second Latin American Conference on Complex Networks (LANET)*, August 2019, Cartagena - Colombia, Proceedings
  URL `https://lanet2019.uniandes.edu.co/wp-content/uploads/proceeding-FINAL.pdf`.
- D. Angulo-García, C. C. Galindo-González, G. Osorio, and D. E. Cermeño-Pinzón, "Assessing resilience of the Colombian Power Grid through percolation analysis", *Second Latin American Conference on Complex Networks (LANET)*, August 2019, Cartagena - Colombia, Proceedings
  URL `https://lanet2019.uniandes.edu.co/wp-content/uploads/proceeding-FINAL.pdf`.

A. About the Practical Use of the Kuramoto Model

This work has presented a simplified model of a power grid that is very popular in the physics community, which focuses on the study of emerging collective behaviour of oscillators and subsequently ignores some of the practical insights of the power system itself. This appendix summarizes some important details found in [4].

In particular, the dynamical model of equation (2-45) can be expressed in a more general form:

$$\frac{2H_j}{\Omega}\ddot{\theta}_{j(t)} + \frac{D_j}{\Omega}\dot{\theta}_{j(t)} = \hat{P}_j + \sum_{i}^{N} K_{ji}\sin(\theta_{i(t)} - \theta_{j(t)} - \gamma_{ij}) \tag{A-1}$$

where H_j and D_j are the inertia and damping constants that describe each machine, respectively. Three distinct models can be defined, all of them describe the dynamics in generators as the second-order oscillators in equation (A-1) but they differ on how the loads are modeled:

- **Synchronous motor model (SM):** Loads are also described as second-order oscillators. In the final topology of the network, every node is connected to every other node.
- **Structure-preserving model (SP):** Loads are described by first-order oscillators ($H_j = 0$) and generators have an additional node connecting it to the rest of the network.
- **Effective network (EN):** Loads are described by constant impedances. This model focuses then just in synchronization of generators.

In [4] a complete algorithm is described to transform a circuit representation of a power system into a graph with either the SM, SP or EN model, which can then be analysed in the synchronization framework.

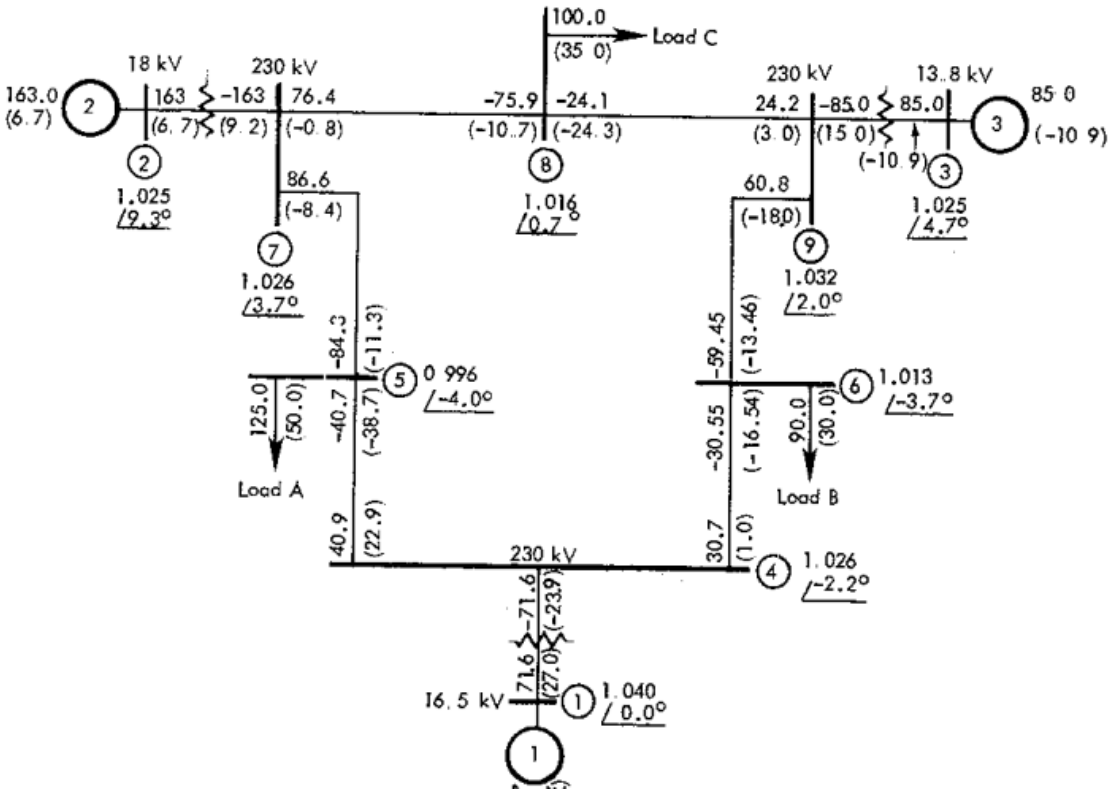

(a) Nine-bus power system.

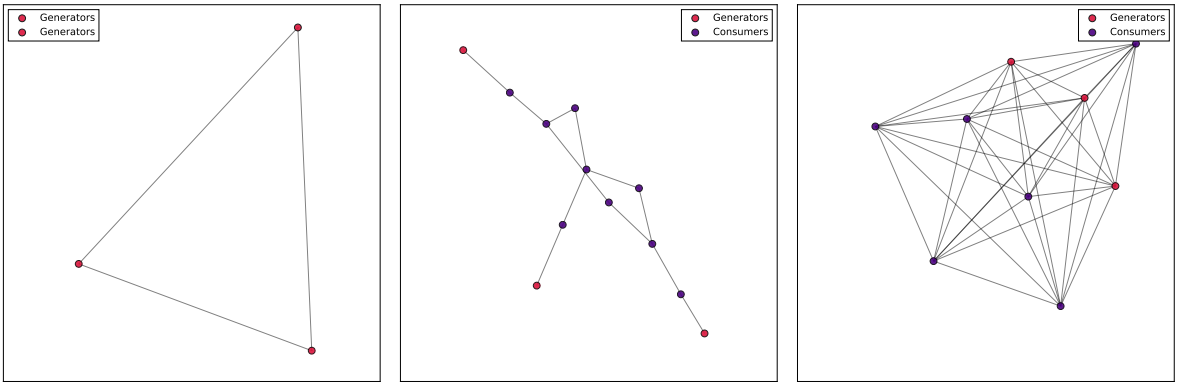

(b) EN model. (c) SP model. (d) SM model.

Figure A-1.: Nine-bus power system and its graph equivalent through the algorithm presented in [4].

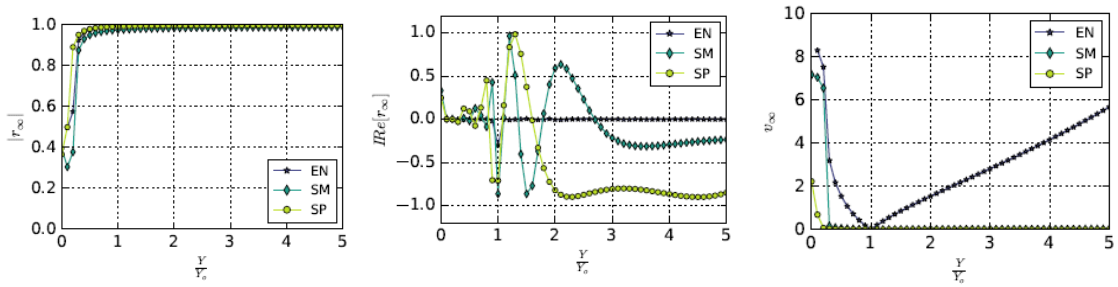

(a) Magnitude of the order parameter. (b) Real part of the order parameter. (c) Average steady state speed.

Figure A-2.: Synchronization in the nine-bus system based on the three reduced models assuming no ohmic loss.

As an example, consider the classic nine-bus system from [65]. Figure **A-1** shows the circuit of the power system and the corresponding graph for either of the three models mentioned. Figure **A-2** shows the results of synchronization for variations in the coupling strength in the nine-bus system with no ohmic loss. It is shown that the EN model could not be studied in the same way as the others, this is to be expected since the only oscillators in the graph are generators, thus equation (2-47) for power balance is not satisfied and the synchronized state can't be assumed to be on zero frequency. Interestingly, both SP and SM models exhibit the transition to synchronization in roughly the same critical point.

The approach taken in this work, and the one which is usually employed in the physics community is the one described in chapter 2, where both, consumers and producers are second-order oscillators as in the SM model, but the structure of the graph is conserved as in the SP model.

B. About Numerical Set Up

B.1. Basin Stability Computation

Computing the single-node basin stability is a computationally intensive task, so to reduce simulation time, virtual machines with multiple CPU cores were used. Operating in parallel, each core calculates the SNBS for one node in the network, thus it runs sequentially multiple time-domain simulations, which are solved through the variable-coefficient ODE solver (VODE) using the backward differentiation formulas (BDF) method, implemented in `scipy`.

Time-domain simulations are performed in a time span of 200 time units and the initial 90 % of them are assumed to be transient dynamics and thus discarded. A trajectory is considered to belong to the basin of attraction if $\| \sum_i^N \dot{\theta}_i \|_2 \leq 0.01$. All these numerical parameters were carefully tuned to allow a fast and sufficiently precise computation.

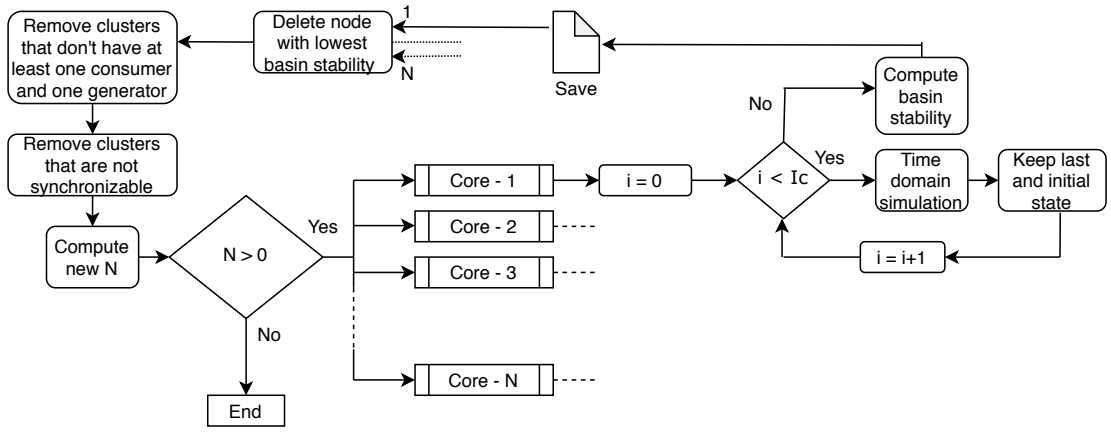

Figure B-1.: Resilience testing algorithm based on single node basin stability.

The resilience assessment algorithm based on SNBS is even more time-consuming since it requires to calculate the SNBS for (almost) every node in every removal iteration. For a clearer interpretation, figure **B-1** shows the basic functioning of the algorithm. These simulations were thus performed on just 50 initial conditions for the time-domain runs. Note that,

randomly sampling points inside or outside the basin of attraction is a repeated Bernoulli experiment [30] and thus follows an absolute standard error $E = \sqrt{S_B(1-S_B)}/\sqrt{I_C}$; which in this case, yields an acceptable maximum error margin of $E \approx 0.071$.

For the detailed analysis of the Colombian power grid shown in section 5.2, 500 initial conditions were executed for each node, leading to an error of $E \approx 0.022$.

On `github.com/ccgalindog`, open source Python implementations for the following algorithms can be found:

- Random growth model for synthetic power grids (section 2.4).
- Tree-like node classification (section 2.5).
- Synchronization tests on regular, random and small-world graphs (section 3.4).
- Single-node basin stability and recovery time calculation (section 5.2).
- Resilience assessment (section 4.2).
- Transformation of PyPower / MatPower cases into SM, SP or EN graphs (appendix A).

Bibliografía

[1] Hypernet_Labs, "Galileo." https://hypernetlabs.io/galileo/, 2020.

[2] P. Schultz, J. Heitzig, and J. Kurths, "A random growth model for power grids and other spatially embedded infrastructure networks," *European Physical Journal: Special Topics*, vol. 223, no. 12, pp. 2593–2610, 2014.

[3] J. Nitzbon, P. Schultz, J. Heitzig, J. Kurths, and F. Hellmann, "Deciphering the imprint of topology on nonlinear dynamical network stability," *New Journal of Physics*, vol. 19, no. 3, 2017.

[4] T. Nishikawa and A. E. Motter, "Comparative analysis of existing models for power-grid synchronization," *New Journal of Physics*, vol. 17, 2015.

[5] A. Pikovsky, M. G. Rosenblum, and J. Kurths, *Synchronization, A Universal Concept in Nonlinear Sciences*. Cambridge: Cambridge University Press, 2001.

[6] A. Arenas, A. Díaz-Guilera, J. Kurths, Y. Moreno, and C. Zhou, "Synchronization in complex networks," *Physics Reports*, vol. 469, no. 3, pp. 93 – 153, 2008.

[7] G. V. Osipov, J. Kurths, and C. Zhou, *Synchronization in oscillatory networks*. Berlin, Germany: Springer, 2007.

[8] F. Dorfler, M. Chertkov, and F. Bullo, "Synchronization in complex oscillator networks and smart grids," *Proceedings of the National Academy of Sciences*, vol. 110, no. 6, pp. 2005–2010, 2013.

[9] A. E. Motter, S. A. Myers, M. Anghel, and T. Nishikawa, "Spontaneous synchrony in power-grid networks," *Nature Physics*, vol. 9, no. 3, pp. 191–197, 2013.

[10] H. Sakaguchi and T. Matsuo, "Cascade Failure in a Phase Model of Power Grids," vol. 81, pp. 1–7, 2012.

[11] S. V. Buldyrev, R. Parshani, G. Paul, H. E. Stanley, and S. Havlin, "Catastrophic cascade of failures in interdependent networks," *Nature*, vol. 464, no. 7291, pp. 1025–1028, 2010.

[12] D. Teather, "Blackout cost New York $36m an hour," *The Guardian*, 2003.

[13] P. Brockway, A. Owen, L. I. Brand Correa, and L. Hardt

[14] K. Xi, J. L. A. Dubbeldam, H. X. Lin, and J. H. V. Schuppen, "Power-Imbalance Allocation Control of Power Systems-Secondary Frequency Control," *Automatica*, vol. 92, pp. 70–72, 2018.

[15] S. Tamrakar, M. Conrath, and S. Kettemann, "Propagation of disturbances in AC electricity grids," *Scientific Reports*, vol. 8, no. 1, pp. 1–11, 2018.

[16] "La revolución renovable que hay en Colombia," *Semana*, 2019.

[17] D. J. Hill and Guanrong Chen, "Power systems as dynamic networks," in *2006 IEEE International Symposium on Circuits and Systems*, pp. 4 pp.–725, 2006.

[18] C. D. Brummitt, P. D. H. Hines, I. Dobson, C. Moore, and R. M. D'Souza, "Transdisciplinary electric power grid science," *Proceedings of the National Academy of Sciences*, vol. 110, no. 30, pp. 12159–12159, 2013.

[19] G. Filatrella, A. H. Nielsen, and N. F. Pedersen, "Analysis of a power grid using a Kuramoto-like model," *European Physical Journal B*, vol. 61, no. 4, pp. 485–491, 2008.

[20] Y. Kuramoto, "Self-entrainment of a population of coupled non-linear oscillators," in *International Symposium on Mathematical Problems in Theoretical Physics* (H. Araki, ed.), (Berlin, Heidelberg), pp. 420–422, Springer Berlin Heidelberg, 1975.

[21] J. A. Acebrón, L. L. Bonilla, C. J. Pérez Vicente, F. Ritort, and R. Spigler, "The kuramoto model: A simple paradigm for synchronization phenomena," *Rev. Mod. Phys.*, vol. 77, pp. 137–185, Apr 2005.

[22] F. Dorfler and F. Bullo, "On the Critical Coupling for Kuramoto Oscillators," pp. 1–27, 2010.

[23] M. Rohden, A. Sorge, D. Witthaut, and M. Timme, "Impact of network topology on synchrony of oscillatory power grids," vol. 013123, pp. 0–8, 2013.

[24] M. Rohden, A. Sorge, M. Timme, and D. Witthaut, "Self-organized synchronization in decentralized power grids," *Physical Review Letters*, vol. 109, no. 6, pp. 1–5, 2012.

[25] S. Olmi, A. Navas, S. Boccaletti, and A. Torcini, "Hysteretic transitions in the Kuramoto model with inertia," *Physical Review E - Statistical, Nonlinear, and Soft Matter Physics*, vol. 90, no. 4, pp. 1–16, 2014.

[26] F. A. Rodrigues, T. K. Peron, P. Ji, and J. Kurths, "The Kuramoto model in complex networks," *Physics Reports*, vol. 610, pp. 1–98, 2016.

[27] H. . Chiang, F. F. Wu, and P. P. Varaiya, "Foundations of the potential energy boundary surface method for power system transient stability analysis," *IEEE Transactions on Circuits and Systems*, vol. 35, no. 6, pp. 712–728, 1988.

[28] H. Kwatny, L. Bahar, and A. Pasrija, "Energy-like lyapunov functions for power system stability analysis," *IEEE Transactions on Circuits and Systems*, vol. 32, no. 11, pp. 1140–1149, 1985.

[29] K. Xi, J. L. Dubbeldam, and H. X. Lin, "Synchronization of cyclic power grids: Equilibria and stability of the synchronous state," *Chaos*, vol. 27, no. 1, 2017.

[30] P. J. Menck, J. Heitzig, N. Marwan, and J. Kurths, "How basin stability complements the linear-stability paradigm," *Nature Physics*, vol. 9, no. 2, pp. 89–92, 2013.

[31] P. J. Menck, J. Heitzig, J. Kurths, and H. J. Schellnhuber, "How dead ends undermine power grid stability," *Nature Communications*, vol. 5, pp. 1–8, 2014.

[32] C. Mitra, A. Choudhary, S. Sinha, J. Kurths, and R. V. Donner, "Multiple-node basin stability in complex dynamical networks," *Physical Review E*, vol. 95, no. 3, pp. 1–9, 2017.

[33] C. Mitra, T. Kittel, A. Choudhary, J. Kurths, and R. V. Donner, "Recovery time after localized perturbations in complex dynamical networks Recovery time after localized perturbations in complex dynamical networks," 2017.

[34] M. F. Wolff, P. G. Lind, and P. Maass, "Power grid stability under perturbation of single nodes: Effects of heterogeneity and internal nodes," *Chaos: An Interdisciplinary Journal of Nonlinear Science*, vol. 28, no. 10, p. 103120, 2018.

[35] P. Schultz, J. Heitzig, and J. Kurths, "Detours around basin stability in power networks," *New Journal of Physics*, vol. 16, 2014.

[36] A. Plietzsch, P. Schultz, J. Heitzig, and J. Kurths, "Local vs. global redundancy – trade-offs between resilience against cascading failures and frequency stability," *European Physical Journal: Special Topics*, vol. 225, no. 3, pp. 551–568, 2016.

[37] A. N. Montanari, E. I. Moreira, and L. A. Aguirre, "Effects of network heterogeneity and tripping time on the basin stability of power systems," *Communications in Nonlinear Science and Numerical Simulation*, vol. 89, p. 105296, 2020.

[38] M. Tyloo, L. Pagnier, and P. Jacquod, "The key player problem in complex oscillator networks and electric power grids: Resistance centralities identify local vulnerabilities," *Science Advances*, vol. 5, no. 11, 2019.

[39] M. Tyloo and P. Jacquod, "Global robustness versus local vulnerabilities in complex synchronous networks," *Phys. Rev. E*, vol. 100, p. 032303, Sep 2019.

[40] F. Hellmann, P. Schultz, P. Jaros, R. Levchenko, T. Kapitaniak, J. Kurths, and Y. Maistrenko, "Network-induced multistability through lossy coupling and exotic solitary states," *Nature Communications*, vol. 11, p. 592, Jan 2020.

[41] M. Tyloo, R. Delabays, and P. Jacquod, "Noise-induced desynchronization and stochastic escape from equilibrium in complex networks," *Phys. Rev. E*, vol. 99, p. 062213, Jun 2019.

[42] I. Simonsen, L. Buzna, K. Peters, S. Bornholdt, and D. Helbing, "Transient dynamics increasing network vulnerability to cascading failures," *Physical Review Letters*, vol. 100, no. 21, pp. 1–4, 2008.

[43] M. Rohden, D. Jung, S. Tamrakar, and S. Kettemann, "Cascading failures in ac electricity grids," *Physical Review E*, vol. 94, no. 3, pp. 1–8, 2016.

[44] B. Schäfer, D. Witthaut, M. Timme, and V. Latora, "Dynamically induced cascading failures in power grids," *Nature Communications*, vol. 9, no. 1, 2018.

[45] M. Fazlyab, F. Dörfler, and V. M. Preciado, "Optimal network design for synchronization of coupled oscillators," *Automatica*, vol. 84, pp. 181 – 189, 2017.

[46] H. Taher, S. Olmi, and E. Schöll, "Enhancing power grid synchronization and stability through time-delayed feedback control," *Phys. Rev. E*, vol. 100, p. 062306, Dec 2019.

[47] S. Dietrich and A. Amnon, "Introduction to percolation theory," 1994.

[48] W. Chen, Z. Zheng, and R. M. D'Souza, "Deriving an underlying mechanism for discontinuous percolation," *Epl*, vol. 100, no. 6, pp. 1–6, 2012.

[49] R. M. D'Souza and M. Mitzenmacher, "Local cluster aggregation models of explosive percolation," *Physical Review Letters*, vol. 104, no. 19, pp. 10–13, 2010.

[50] Z. Kong and E. M. Yeh, "Correlated and cascading node failures in random geometric networks: A percolation view," *ICUFN 2012 - 4th International Conference on Ubiquitous and Future Networks, Final Program*, vol. 56, no. 11, pp. 520–525, 2012.

[51] H. Xiao and E. M. Yeh, "Cascading link failure in the power grid: A percolation-based analysis," *IEEE International Conference on Communications*, 2011.

[52] L. A. Machuca Moreno, "Análisis de estabilidad transitoria basado en teoría de redes complejas y el fenómeno de percolación," 2017.

[53] M. Mureddu, G. Caldarelli, A. Damiano, A. Scala, and H. Meyer-Ortmanns, "Islanding the power grid on the transmission level: less connections for more security," *Scientific Reports*, vol. 6, p. 34797, Oct 2016.

[54] J. Gao, X. Liu, D. Li, and S. Havlin, "Recent progress on the resilience of complex networks," *Energies*, vol. 8, no. 10, pp. 12187–12210, 2015.

[55] D. H. Kim, D. A. Eisenberg, Y. H. Chun, and J. Park, "Network topology and resilience analysis of south korean power grid," *Physica A: Statistical Mechanics and its Applications*, vol. 465, pp. 13 – 24, 2017.

[56] C. Fu, Y. Gao, S. Cai, H. Yang, and C. Yang, "Center of mass in complex networks," *Scientific Reports*, vol. 7, no. December 2016, pp. 1–7, 2017.

[57] R. V. Solé, M. Rosas-Casals, B. Corominas-Murtra, and S. Valverde, "Robustness of the european power grids under intentional attack," *Phys. Rev. E*, vol. 77, p. 026102, Feb 2008.

[58] D. Li, Q. Zhang, E. Zio, S. Havlin, and R. Kang, "Network reliability analysis based on percolation theory," *Reliability Engineering and System Safety*, vol. 142, pp. 556–562, 2015.

[59] L. Chen, P. Ji, D. Waxman, W. Lin, and J. Kurths, "Effects of dynamical and structural modifications on synchronization," *Chaos: An Interdisciplinary Journal of Nonlinear Science*, vol. 29, no. 8, p. 083131, 2019.

[60] Z. Huang, C. Wang, S. Ruj, M. Stojmenovic, and A. Nayak, "Modeling cascading failures in smart power grid using interdependent complex networks and percolation theory," *Proceedings of the 2013 IEEE 8th Conference on Industrial Electronics and Applications, ICIEA 2013*, pp. 1023–1028, 2013.

[61] Y. Yang and A. E. Motter, "Cascading failures as continuous phase-space transitions," *Phys. Rev. Lett.*, vol. 119, p. 248302, Dec 2017.

[62] C. Caro-Ruiz, J. Ma, D. Hill, A. Pavas, and E. Mojica-Nava, "A minimum cut-set vulnerability analysis of power networks," *Sustainable Energy, Grids and Networks*, vol. 21, p. 100302, 2020.

[63] J. Saramäki, M. Kivelä, J. P. Onnela, K. Kaski, and J. Kertész, "Generalizations of the clustering coefficient to weighted complex networks," *Physical Review E - Statistical, Nonlinear, and Soft Matter Physics*, vol. 75, no. 2, pp. 1–4, 2007.

[64] U. Brandes, "A faster algorithm for betweenness centrality," *The Journal of Mathematical Sociology*, vol. 25, no. 2, pp. 163–177, 2001.

[65] P. M. Anderson and A. A. Fouad, *Power system control and stability*. 2002.

[66] K. Schmietendorf, J. Peinke, R. Friedrich, and O. Kamps, "Self-organized synchronization and voltage stability in networks of synchronous machines," *European Physical Journal: Special Topics*, vol. 223, no. 12, pp. 2577–2592, 2014.

[67] Y. Kuramoto, *Chemical oscillations, waves, and turbulence*. 2003.

[68] S. H. Strogatz, "From Kuramoto to Crawford: Exploring the onset of synchronization in populations of coupled oscillators," *Physica D: Nonlinear Phenomena*, vol. 143, no. 1-4, pp. 1–20, 2000.

[69] S. Strogatz, *SYNC: The emerging science of spontaneous order*. 2003.

[70] P. Ji, T. K. D. M. Peron, F. A. Rodrigues, and J. Kurths, "Low-dimensional behavior of Kuramoto model with inertia in complex networks," *Scientific Reports*, vol. 4, pp. 1–6, 2014.

[71] B. Sonnenschein, T. K. Peron, F. A. Rodrigues, J. Kurths, and L. Schimansky-Geier, "Collective dynamics in two populations of noisy oscillators with asymmetric interactions," *Physical Review E - Statistical, Nonlinear, and Soft Matter Physics*, vol. 91, no. 6, pp. 1–7, 2015.

[72] M. Rohden, D. Witthaut, M. Timme, and H. Meyer-Ortmanns, "Curing critical links in oscillator networks as power grid models," *Submitted*, no. December, pp. 0–10, 2015.

[73] H. Kim, S. H. Lee, and P. Holme, "Building blocks of the basin stability of power grids," *Physical Review E*, vol. 93, no. 6, pp. 1–8, 2016.

[74] L. Cao, C. Tian, Z. Wang, X. Zhang, and Z. Liu, "Influence of stochastic perturbations on the cluster explosive synchronization of second-order Kuramoto oscillators on networks," *Physical Review E*, vol. 022220, pp. 1–7, 2018.

[75] J. M. Grzybowski, E. E. Macau, and T. Yoneyama, "On synchronization in power-grids modelled as networks of second-order Kuramoto oscillators," *Chaos*, vol. 26, 2016.

[76] A. B. Birchfield, E. Schweitzer, M. H. Athari, T. Xu, T. J. Overbye, A. Scaglione, and Z. Wang, "A metric-based validation process to assess the realism of synthetic power grids," *Energies*, vol. 10, no. 8, 2017.

[77] A. S. Eran Schweitzer and R. Thomas, "The validation of synthetic power system cases," *IREP'2017 Symposium*, 2017.

[78] Z. Liu, Y. Zhang, Y. Wang, N. Wei, and C. Gu, "Development of the interconnected power grid in europe and suggestions for the energy internet in china," *Global Energy Interconnection*, vol. 3, no. 2, pp. 111 – 119, 2020.

[79] S. H. Yook and H. Meyer-Ortmanns, "Synchronization of Rössler oscillators on scale-free topologies," *Physica A: Statistical Mechanics and its Applications*, vol. 371, no. 2, pp. 781–789, 2006.

[80] T. Nishikawa, A. E. Motter, Y. C. Lai, and F. C. Hoppensteadt, "Heterogeneity in Oscillator Networks: Are Smaller Worlds Easier to Synchronize?," *Physical Review Letters*, vol. 91, no. 1, pp. 2–5, 2003.

[81] A. G. H. (auth.), *Percolation Theory For Flow In Porous Media*. Lecture Notes in Physics 674, Springer Berlin Heidelberg, 1 ed., 2005.

[82] R. Carareto, M. S. Baptista, and C. Grebogi, "Natural synchronization in power-grids with anti-correlated units," *Communications in Nonlinear Science and Numerical Simulation*, vol. 18, no. 4, pp. 1035–1046, 2013.

[83] D. Witthaut and M. Timme, "Braess's paradox in oscillator networks, desynchronization and power outage," *New Journal of Physics*, vol. 14, pp. 1–17, 2012.

[84] E. B. T. Tchuisseu, D. Gomila, P. Colet, D. Witthaut, M. Timme, and B. Schäfer, "Curing braess' paradox by secondary control in power grids," *New Journal of Physics*, vol. 20, no. 8, pp. 1–11, 2018.

[85] J. P. Pade and T. Pereira, "Improving Network Structure can lead to Functional Failures," *Nature Publishing Group*, pp. 1–6, 2015.

[86] R. S. Pinto and A. Saa, "Synchrony-optimized networks of Kuramoto oscillators with inertia," *Physica A: Statistical Mechanics and its Applications*, vol. 463, pp. 77–87, 2016.

[87] M. Fazlyab, F. Dörfler, and V. M. Preciado, "Optimal network design for synchronization of coupled oscillators," *Automatica*, vol. 84, pp. 181–189, 2017.

[88] H. Kim, S. H. Lee, J. Davidsen, and S.-w. Son, "Multistability and variations in basin of attraction in power-grid systems," 2018.

[89] T. Coletta, R. Delabays, I. Adagideli, and P. Jacquod, "Topologically protected loop flows in high voltage AC power grids This,"

[90] Wei Wu and Chikong Wong, "Facts applications in preventing loop flows in interconnected systems," in *2003 IEEE Power Engineering Society General Meeting (IEEE Cat. No.03CH37491)*, vol. 1, pp. 170–174 Vol. 1, 2003.

[91] P. Schultz, P. J. Menck, J. Heitzig, and J. Kurths, "Potentials and limits to basin stability estimation," *New Journal of Physics*, vol. 19, p. 023005, feb 2017.

[92] M. Khedkar, G. Dhole, and V. Neve, "Transient stability analysis by transient energy function method: Closest and controlling unstable equilibrium point approach," *Journal of the Institution of Engineers (India): Electrical Engineering Division*, vol. 85, pp. 83–88, 09 2004.

[93] H.-D. Chang, C.-C. Chu, and G. Cauley, "Direct stability analysis of electric power systems using energy functions: Theory, applications, and perspective," *Proceedings of the IEEE*, vol. 83, pp. 1497 – 1529, 12 1995.

[94] F. Hellmann, P. Schultz, C. Grabow, J. Heitzig, and J. Kurths, "Survivability of Deterministic Dynamical Systems," *Scientific Reports*, vol. 6, no. March, pp. 1–12, 2016.

[95] UPME, *STN - Sistema de Transmisión Nacional de Energía Eléctrica, Colombia, http://sig.simec.gov.co/GeoPortal/Mapas/Mapas*, 2016.